



Utility of an image-based canopy reflectance modeling tool for remote estimation of LAI and leaf chlorophyll content at the field scale

Rasmus Houborg*, Martha Anderson, Craig Daughtry

USDA-ARS Hydrology and Remote Sensing Laboratory, Beltsville, MD, United States

ARTICLE INFO

Article history:

Received 25 January 2008

Received in revised form 25 September 2008

Accepted 27 September 2008

Keywords:

Leaf chlorophyll

Canopy reflectance

Image-based application

Corn

Leaf area index

Green reflectance

Vegetation stress

Inverse modeling

Look-up tables

Leaf optics

Atmospheric radiative transfer

Regularization

Satellite

ABSTRACT

This paper presents a physically-based approach for estimating critical variables describing land surface vegetation canopies, relying on remotely sensed data that can be acquired from operational satellite sensors. The REGularized canopy reFLECtance (REGFLEC) modeling tool couples leaf optics (PROSPECT), canopy reflectance (ACRM), and atmospheric radiative transfer (6SV1) model components, facilitating the direct use of at-sensor radiances in green, red and near-infrared wavelengths for the inverse retrieval of leaf chlorophyll content (C_{ab}) and total one-sided leaf area per unit ground area (LAI). The inversion of the canopy reflectance model is constrained by assuming limited variability of leaf structure, vegetation clumping, and leaf inclination angle within a given crop field and by exploiting the added radiometric information content of pixels belonging to the same field. A look-up-table with a suite of pre-computed spectral reflectance relationships, each a function of canopy characteristics, soil background effects and external conditions, is accessed for fast pixel-wise biophysical parameter retrievals. Using 1 m resolution aircraft and 10 m resolution SPOT-5 imagery, REGFLEC effectuated robust biophysical parameter retrievals for a corn field characterized by a wide range in leaf chlorophyll levels and intermixed green and senescent leaf material. Validation against in-situ observations yielded relative root-mean-square deviations (RMSD) on the order of 10% for the 1 m resolution LAI (RMSD=0.25) and C_{ab} (RMSD=4.4 $\mu\text{g cm}^{-2}$) estimates, due in part to an efficient correction for background influences. LAI and C_{ab} retrieval accuracies at the SPOT 10 m resolution were characterized by relative RMSDs of 13% (0.3) and 17% (7.1 $\mu\text{g cm}^{-2}$), respectively, and the overall intra-field pattern in LAI and C_{ab} was well established at this resolution. The developed method has utility in agricultural fields characterized by widely varying distributions of model variables and holds promise as a valuable operational tool for precision crop management. Work is currently in progress to extend REGFLEC to regional scales.

Published by Elsevier Inc.

1. Introduction

Remotely sensed data in the reflective optical domain function as a unique cost-effective source for providing spatially and temporally distributed information on key biophysical and biochemical parameters of land surface vegetation. Leaf area index (LAI), defined as the single sided leaf area per unit horizontal ground area, is a critical structural variable for understanding biophysical processes of vegetation canopies and for quantifying exchange processes of energy and matter between the land surface and lower atmosphere (Moran et al., 1995; Norman et al., 1995; Anderson et al., 2005; Doraiswamy et al., 2004). Measurements of total leaf chlorophyll content (C_{ab}), defined as the sum of the contents of chlorophyll *a* and chlorophyll *b* per unit leaf area, can assist in determining photosynthetic capacity and productivity (Boegh et al., 2002; Gitelson et al., 2006; Nijs et al., 1995). Leaf

chlorophyll is a good indicator of vegetation stress (Carter 1994; Penuelas & Filella, 1998; Gitelson & Merzlyak, 1997), it is strongly related to leaf nitrogen content (Filella et al., 1995; Daughtry et al., 2000; Yoder & Pettigrew-Crosby, 1995) and could therefore prove valuable for precision crop management (Moran et al., 1997).

Remote sensing techniques for estimating vegetation characteristics from reflective optical measurements have either been based on the empirical-statistical approach that links vegetation indices (VI) and vegetation parameters using experimental data, or on the inversion of a physical canopy reflectance (CR) model. The empirical approach is simple and computationally efficient, and the potential of empirical VI relationships for the determination of crop parameters has been demonstrated in numerous studies (e.g. Broge & Mortensen, 2002; Colombo et al., 2003; Gitelson et al., 2005; Tucker, 1980). However, a fundamental problem with the VI approach is its lack of generality. The shape and form of canopy reflectance spectra depend on a complex interaction of several internal (e.g. vegetation structure, leaf biochemical composition, soil background) and external (e.g. view-sun-target geometry, atmospheric state) factors (Baret, 1991)

* Corresponding author.

E-mail address: rasmus.houborg@ars.usda.gov (R. Houborg).

that may vary significantly in time and space and from one crop type to another. As a consequence, there is no unique relationship between a sought vegetation parameter and a VI of choice, but rather a family of relationships, each a function of canopy characteristics, soil background effects and external conditions (Baret & Guyot, 1991; Colombo et al., 2003; Gobron et al., 1997; Haboudane et al., 2004; Houborg et al., 2007a; Zarco-Tejada et al., 2003).

Physically-based models have proven to be a promising alternative as they describe the transfer and interaction of radiation inside the canopy based on physical laws and thus provide an explicit connection between the biophysical variables and the canopy reflectance. Different strategies have been proposed for the inversion of these models including iterative numerical optimization methods (e.g. Jacquemoud et al., 1995, 2000), look-up table approaches (e.g. Combal et al., 2002a; Knyazikhin et al., 1998; Weiss et al., 2000) and artificial neural network methods (e.g. Bacour et al., 2006; Fang & Liang, 2005; Walthall et al., 2004; Weiss & Baret, 1999); each associated with specific advantages and disadvantages (Kimes et al., 2000). The iterative optimization approach facilitates a direct retrieval of biophysical parameters from observed reflectances without the use of calibration or training data of any kind, and Houborg and Boegh (2008) presented a way to make this kind of inversion computationally feasible at local to regional scales.

The inversion process is ill-posed by nature due to measurements and model uncertainties and because different combinations of model parameters may correspond to almost identical spectra (Combal et al., 2002a; Atzberger, 2004). As a result, additional information is needed to accurately estimate the vegetation parameters. While the use of a priori knowledge (e.g. canopy type and architecture, model parameter ranges) has been shown to be an efficient way to solve ill-posed inverse problems (Combal et al., 2002a, 2002b; Koetz et al., 2005; Qu et al., 2007), this regularization technique typically relies on the existence of experimental data collected at the site of interest. Using multiple MODIS images, Houborg et al. (2007a) demonstrated how the temporal evolution of LAI could be utilized as another way of regularizing the inverse problem. Atzberger (2004) proposed an entirely image-based regularization technique that incorporates radiometric information from neighboring pixels during model inversion. It was shown that the so-called “object signatures” contained real supplementary information, which helped to regularize the inverse problem (Atzberger, 2004). Houborg and Boegh (2008) reported good LAI and C_{ab} retrieval accuracies using a related image-based regularization strategy that assumed invariance of dry matter content, vegetation clumping and leaf angle distribution within well-defined land cover classes.

This paper proposes a number of important refinements to the biophysical parameter retrieval scheme described in Houborg and Boegh (2008). The focus here is on the field-scale applicability of the refined model whereas a future paper will evaluate the model utility at regional scales. In the original model, the atmospheric correction of the sensor radiances was performed independent of the CR modeling assuming Lambertian reflectance of the land surface. In reality, surface anisotropic effects can be significant (Kimes & Sellers, 1985) and the atmospheric correction should take into account these non-Lambertian surface boundary conditions to be consistent with the directional canopy reflectance spectra required as input to a multidirectional CR model (Verhoef & Bach, 2003). This is addressed here by coupling the PROSPECT leaf optics model (Baret & Fourty, 1997; Jacquemoud & Baret, 1990) and the turbid medium Markov chain canopy reflectance model, ACRM (Kuusk 1995, 2001) with a vector version of the 6S (Second Simulation of the Satellite Signal in the Solar Spectrum) atmospheric radiative transfer model (6SV1) (Kotchenova et al., 2006; Vermote et al., 1997). Another improvement accommodates partially senescent vegetation. Canopies of exclusively green leaves were assumed in Houborg and Boegh (2008) which will lead to large inaccuracies when applied to a canopy with intermixing of green and senescent leaf material (Bacour et al., 2002a). In this study the spectra of green and senescent leaves are modeled using PROSPECT. The correction for background effects has also

been improved; the methodology presented in Houborg and Boegh (2008) required at least two satellite scenes to represent conditions of dense green vegetation and bare soil, respectively for each land cover class. In the refined model only an approximate first estimate of the background reflectance signal from a nearby bare soil or partially vegetated field is required as input to a novel pixel-wise soil correction scheme, which makes the new model also applicable to mono-temporal imagery. Additionally, prior information about the leaf inclination angle is no longer a prerequisite.

The key objective of this study is to develop a method for reliable biophysical parameter retrievals that 1) is entirely image-based, 2) does not rely on difficult to obtain in-situ measurements, 3) can be applied at a range of scales using radiometric spectral information from different airborne and operational satellite sensor systems, and 4) can be used for agricultural fields characterized by widely varying distributions of model variables. Following Atzberger (2004) and Houborg and Boegh (2008), the radiometric information content of pixels belonging to the same field or land cover class is exploited assuming small intra-field variability of leaf inclination angle distribution, leaf mesophyll structure and Markov clumping characteristics. These field-specific parameters are estimated by an iterative inversion technique using reflectance observations characteristic of intermediate to dense vegetation coverage (Houborg & Boegh, 2008). With the determination of the field-specific parameters completed using regularized inverse modeling, pre-computed look-up tables are accessed for fast pixel-wise parameter estimations. New image-based techniques are introduced to further regularize the inversion and to avoid confounding effects between the soil background reflectance and the canopy variables.

The atmospheric radiative transfer and canopy reflectance models are described in the next two sections followed by a detailed description of the integrated biophysical parameter retrieval tool. To demonstrate the feasibility and reliability of the approach, the tool is applied to a stressed corn field in Maryland, USA using 1 m resolution aerial imagery and 10 m resolution SPOT-5 data. Finally the accuracy of LAI and C_{ab} retrievals is evaluated using in-situ data.

2. Atmospheric radiative transfer model

The vector version of the 6S (Second Simulation of the Satellite Signal in the Solar Spectrum) atmospheric radiative transfer model (6SV1) (Kotchenova et al., 2006; Vermote et al., 1997) is used to convert at-sensor radiance to directional surface reflectance (Section 4). 6SV1 is an advanced radiative transfer code designed to simulate the reflection of solar radiation by a coupled atmosphere-surface system for a wide range of atmospheric, spectral and geometrical conditions. It was selected over competing models (e.g. MODTRAN) as bidirectionally reflecting surface conditions can be considered and the CR model, ACRM (Section 3) is already built-in. The updated 6S code accounts for radiation polarization and includes other significant updates, and has demonstrated good performance (Kotchenova et al., 2006; Kotchenova & Vermote, 2007). Collection 5 of the MODIS surface reflectance dataset was produced using 6SV1 (<http://6s.ltdri.org/>). For the present application, input parameters for 6SV1 include solar and sensor view angle geometries: sun zenith (θ_s), view zenith (θ_v), and relative azimuth (θ_{raz}) angles, total ozone content (O_3), aerosol optical depth at 550 nm (τ_{550}), total precipitable water (TPW), and type of aerosol model (τ_{type}) (Table 1). The type of aerosol model (Continental, Urban, Maritime and Desert) determines the aerosol volume and size distributions, and an option is implemented to allow mixing of aerosol models (Table 1). TPW can be replaced by atmospheric profile data, but an integrated value is generally sufficient especially for this application, as it does not include spectral bands in the water-sensitive mid-infrared wavelength region (Section 4).

Non-Lambertian ground conditions are considered in this implementation of 6SV1. The ground BRDF, required to determine the directional effect of the target, is computed in 6SV1 following the Markov chain

Table 1

Input parameters required to run REGFLEC (see Section 5.2 for a description of the external input parameters)

Parameters	Units	Symbol	Range or fixed value
<i>External/atmospheric parameters</i>			
Aerosol optical depth (at 550 nm)		τ_{550}	0.23
Total precipitable water vapor	g cm ⁻²	TPW	3.51
Total ozone content	cm-atm	O ₃	0.378
Aerosol model		τ_{type}	40,60,0,0 ^a
Sun zenith angle	(°)	θ_s	23.35
Relative azimuth angle	(°)	θ_v	144.1
View zenith angle	(°)	θ_{raz}	22.01
<i>Canopy structure parameters</i>			
Leaf area index		LAI	0–9
Markov clumping parameter		S_z	0.4–1.0
Hot spot parameter		S_L	0.5/LAI
Mean leaf inclination angle	(°)	θ_l	40–70
LAI of the ground level		LAI _g	0.05
Fraction of senescent leaves		f_B	0–1
<i>Soil parameters</i>			
Weight of the first price function		s_1	0.05–0.5
<i>Leaf biochemical constituents</i>			
Chlorophyll <i>a+b</i> content	µg cm ⁻²	C_{ab}	10–90
Leaf equivalent water thickness	cm	C_w	0.02
Dry matter content	g m ⁻²	C_m	50
Brown pigments		C_{bp}	0, 3 ^b
Leaf mesophyll structure		N	1–2.5

For the initial 6SV1 run, the ground BRDF was calculated by parameterizing the canopy parameters as the midpoints of the effective ranges.

^a For the aerosol model (τ_{type}), the values [40,60,0,0] indicate the percentage of aerosols characterized by Continental, Urban, Maritime and Desert aerosol size/type distributions, respectively.

^b $C_{bp}=0$: green leaves (no light absorption by brown pigments), $C_{bp}=3$: represents yellow leaves.

canopy reflectance model, ACRM (Kuusk 1995, 2001) (Section 3). The consideration of directional effects is believed to be important due to significant non-Lambertian scattering properties of vegetation surfaces (Kimes & Sellers, 1985) and the directional influence of many model parameters on the canopy reflectance (Bacour et al., 2002a). Additionally, key vegetation parameters like leaf chlorophyll change due to relatively subtle differences in canopy reflectance (e.g. Daughtry et al., 2000).

3. Canopy reflectance model

The turbid medium Markov chain canopy reflectance model, ACRM (Kuusk 1995, 2001) incorporates Markov properties of stand geometry making it applicable to plant canopies largely made up of vertical elements such as corn (Kuusk, 1995). ACRM assumes the canopy consists of a homogeneous layer of vegetation and a thin layer of vegetation on the ground surface. The model operates in the spectral domain 400–2500 nm and calculates directional canopy reflectance at a spectral resolution of 1 nm. The model inputs are listed in Table 1. The angular distribution of leaves is described by the model leaf inclination (θ_m) and the eccentricity (e_L) in accordance with an elliptical leaf angle distribution (LAD). However as a simplification, the mean leaf inclination angle (θ_l) is used in this study to parameterize both θ_m and e_L in accordance with an ellipsoidal LAD (Campbell, 1990), which implies considering only planophile and erectophile model leaf orientations ($\theta_m=0$ and $\theta_m=90$, respectively). The Markov clumping parameter (S_z) was set to vary between a value of 0.4, representing a significantly clumped plant canopy, and 1.0, representing a homogeneous canopy of randomly positioned leaves. The model accounts for non-Lambertian soil reflectance and soil reflectance spectra are approximated as a function of four basis vectors, which were sufficient to describe the spectral variability of reflectance spectra from more than 500 soils (Price, 1990). In REGFLEC, however, the third and fourth vectors are set equal to zero and the second vector

is tied to the first vector (s_1), which explains most of the spectral variability in the soil reflectance (Price, 1990). Additionally, the specular reflection of direct solar radiation of leaves and the hot spot effect are accounted for. Since the model sensitivity to the hot spot parameter, S_L , is generally very low for view directions away from the hot spot direction (Bacour et al., 2002b), it was roughly parameterized as a function of LAI according to Verhoef and Bach (2003). The ACRM calculation of the relative proportion of direct and diffuse flux in incoming radiation was replaced by the wavelength-dependent diffuse fraction computed by 6SV1.

In ACRM, the spectra of leaf reflectance and transmittance are computed using the most recent version of the leaf optics model PROSPECT (Baret & Fourty, 1997; Jacquemoud & Baret, 1990). In this five-variable PROSPECT model, leaf scattering is described by the leaf mesophyll structure parameter N (the effective number of elementary layers inside a leaf) and a tabulated wavelength-dependent refractive index of the leaf surface wax. The calculation of leaf absorption depends on the chlorophyll *a* and *b* content (C_{ab}), the equivalent water thickness (C_w), the dry matter content (C_m), and leaf brown pigment (C_{bp}) (Table 1). The setting of C_w is not important since leaf water has no effect on the reflectance in the visible and near-infrared wavebands (Houborg et al., 2007a). The effect of C_m is predominantly in wavelengths longer than 1200 nm (Botha et al., 2007; Houborg et al., 2007a), and was set to a fixed value of 50 g m⁻² in agreement with the average value obtained during the Leaf Optical Properties Experiment (LOPEX'93) (Hosgood et al., 1995). Brown pigments appear when leaves senesce and represent light absorption by non-chlorophyll pigments. C_{bp} may vary between 0 (no light absorption) and ~6 (max. light absorption). In this study, green and senescent leaf materials were assumed to be dissociated and assigned fixed C_{bp} values of 0 and 3, respectively. The leaf mesophyll structure and leaf chlorophyll content of senescent leaf material were fixed to 2.5 and 0 µg cm⁻², respectively. Reflectance spectra representative of intermixed green and senescent leaf material was then simulated by weighing PROSPECT leaf reflectance and transmittance spectra for green ($C_{bp}=0$) and senescent leaf material ($C_{bp}=3$) with a new input parameter, the canopy fraction of senescent leaves (f_B).

In this study, the inversion of ACRM for the retrieval of two or more model parameters involves minimizing the residuals between observed canopy reflectance (ρ_j^*) and simulated canopy reflectance (ρ_j) according to the merit function:

$$\chi = \sum_{j=1}^m \left(\frac{\rho_j^* - \rho_j}{\varepsilon_j} \right)^2 + \sum w_i \quad (1)$$

Here ε_j is the reflectance uncertainty estimate and m is the number of the measured reflectance values. The second term is included to avoid non-physical values of input parameters (see Table 1 for allowable range values); if the parameter falls within the given boundaries, w_i will have a value of zero, else a penalty value is assigned to w_i . The Powell minimization technique is used to solve the multi-dimensional function (Kuusk, 2003).

4. REGularized canopy reFLECtance modeling tool

The REGularized canopy reFLECtance (REGFLEC) modeling tool (Fig. 1) integrates the atmospheric radiative transfer (Section 2) and leaf optics and canopy reflectance (Section 3) models and combines iterative and look-up table based inversion techniques for the retrieval of key biophysical properties (LAI and C_{ab}). Input parameters to the model include remotely sensed at-sensor radiance observations in green, red, and near-infrared wavelengths, atmospheric state parameters to describe atmospheric scattering and absorption characteristics and solar and sensor view angle geometries (Fig. 1). The REGFLEC retrieval scheme can be described as a 4 step procedure as displayed in Fig. 1 and explained in detail in four separate sections below.

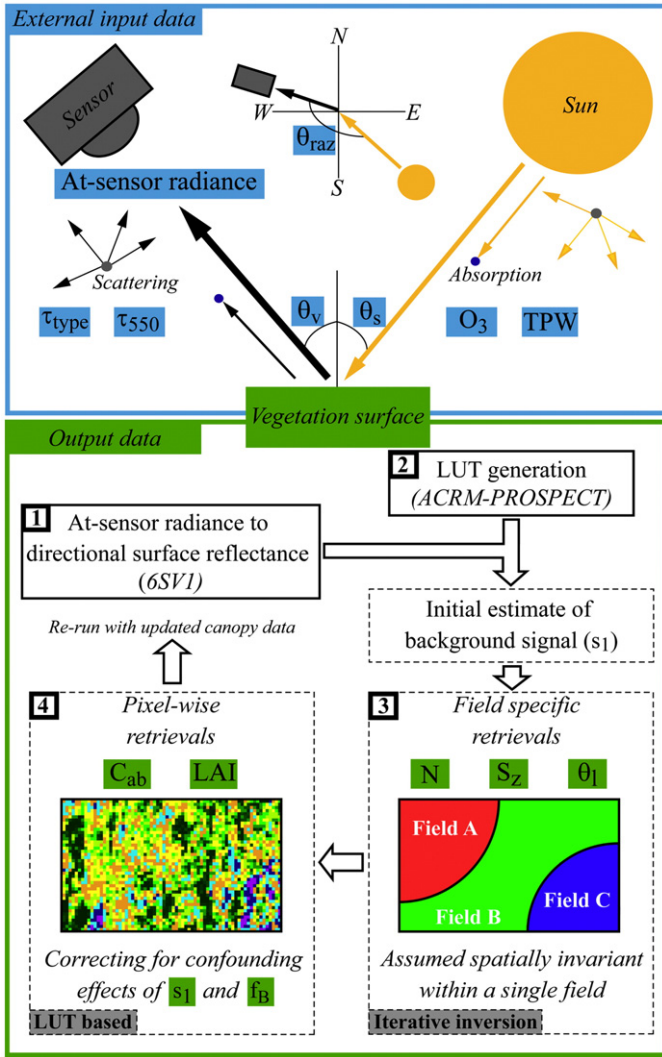


Fig. 1. A schematic diagram of the coupled PROSPECT-ACRM-6SV1 regularized biophysical parameter retrieval tool (REGFLEC). Parameter descriptions are given in the text.

4.1. At-sensor radiance to surface reflectance conversion (step 1)

The first step in REGFLEC (Fig. 1) involves the conversion of at-sensor radiances in green, red and near-infrared wavebands to directional surface reflectance using 6SV1 (Section 2). Since the atmospheric correction routine is coupled to the leaf biochemical and canopy biophysical characteristics of the surface, 6SV1 is re-run after surface characteristics are updated by the inversion process (Fig. 1). For the initial 6SV1 run, ACRM is parameterized with default settings of the input parameters (Table 1), using a nominal value of LAI that is calculated according to Campbell and Norman (1998) as a function of fraction of vegetation cover (f_c) reported by Choudhury et al. (1994) as a function of the normalized difference vegetation index (NDVI)

$$\text{LAI} = -2 \ln(1 - f_c) \quad (2)$$

$$f_c = 1 - \left[\frac{\text{NDVI}_{\max} - \text{NDVI}_i}{\text{NDVI}_{\max} - \text{NDVI}_{\min}} \right]^{0.6}$$

Here NDVI_i is the NDVI of an individual pixel and NDVI_{\max} and NDVI_{\min} are the maximum and minimum NDVI of the image, respectively.

4.2. Look-up table generations (step 2)

Fast pixel-wise mapping operations (Section 4.4) are facilitated using a look-up table (LUT) based inversion approach. The LUTs, generated by running ACRM in forward mode with input of site-specific view-sun angles, contain a suite of simulated $\text{LAI}-\rho_{\text{nir}}$, $\text{LAI}-\text{NDVI}$, $C_{\text{ab}}-\rho_{\text{green}}$, and $f_B-\text{RGVI}$ relationships resembling a wide parameter distribution space (Table 1), where

$$\text{NDVI} = \frac{\rho_{\text{nir}} - \rho_{\text{red}}}{\rho_{\text{nir}} + \rho_{\text{red}}}, \quad \text{RGVI} = \frac{\rho_{\text{red}} - \rho_{\text{green}}}{\rho_{\text{red}} + \rho_{\text{green}}} \quad (3)$$

and ρ_{green} , ρ_{red} and ρ_{nir} represent simulated surface reflectances in green, red and near-infrared wavelengths. The LUTs are multidimensional arrays where the number of dimensions is determined by the number of parameters that have an impact on the given relationship. For instance, $\text{LAI}-\text{NDVI}$ relationships (simulated by ACRM) are impacted by variations in C_{ab} , N , S_z , f_B , θ_1 and s_1 (Houborg et al., 2007a), which make a 7 dimensional $\text{LAI}-\text{NDVI}$ LUT, as a relationship must be stored for all possible combinations of each C_{ab} , N , S_z , f_B , θ_1 and s_1 entry. The $\text{LAI}-\rho_{\text{nir}}$ LUT on the other hand only consists of 6 dimensions as leaf chlorophyll has no effect outside the visible spectrum (Houborg et al., 2007a).

The look-up tables are computed for 16 LAI, 13 C_{ab} and 7 θ_1 values evenly distributed across the parameter ranges (Table 1) in addition to 3 N values (1.0, 1.8, 2.5), 2 S_z values (0.4, 1.0), 3 s_1 values (0.05, 0.3, 0.5) and 6 f_B values (0.0, 0.2, 0.4, 0.6, 0.8, 1.0). The LUTs are only computed for a few entries of the latter four parameters (i.e. N , S_z , s_1 , f_B) to reduce the computational demand of the LUT generation. Values of C_{ab} , N , S_z , f_B , θ_1 and s_1 must be known in order to access LUT stored $\text{LAI}-\text{NDVI}$ relationships. Conversely, knowledge of LAI, N , S_z , f_B , θ_1 and s_1 is required to access LUT stored $C_{\text{ab}}-\rho_{\text{green}}$ relationships. If derived parameter values of N , S_z , s_1 and f_B fall in between their respective LUT parameter entries, the given reflectance relationship (e.g. $\text{LAI}-\text{NDVI}$) is approximated by linearly interpolating between the relationships of the bounding parameter entries. Spectral relationships derived using this interpolation technique were found to closely match relationships simulated directly using ACRM and significantly increased the computational speed.

4.3. Field specific parameter retrievals (step 3)

ACRM is here applied in iterative inverse mode, by minimizing the Eq. (1) merit function, for the estimation of canopy and leaf parameters assumed spatially invariant within a given crop field (i.e. S_z , N and θ_1).

Regularization techniques have been implemented since a simultaneous (pixel-wise) retrieval of ACRM parameters using iterative optimization methods is unfeasible for a number of key reasons: 1) due to the ill-posed nature of model inversion, different parameter settings are likely to yield identical spectra (Weiss et al., 2000; Jacquemoud et al., 2000), especially when several parameters are estimated simultaneously (Kuusk et al., 1997); 2) the expensive computational requirement of iterative numerical optimization methods generally makes pixel-wise parameter retrievals unfeasible (Kimes et al., 2000; Houborg & Boegh, 2008); and 3) the solution is highly dependent on the initial settings of the model parameters, which may result in optimization at a local minimum instead of the global minimum in RMSD between observed and modeled reflectances (Jacquemoud et al., 2000; Botha et al., 2007).

The regularization techniques implemented in REGFLEC include:

- 1) REGFLEC contains an option to include prior knowledge of θ_1 and fix it for the specific field. If this knowledge is unavailable, θ_1 is kept as a free parameter.
- 2) The inversion is run using only the spectral information content from pixels with an intermediate to high vegetation coverage ($\text{NDVI} > 0.65$), thereby maximizing the sensitivity of the reflectance

signal to the leaf and canopy variables while reducing the influence of the background reflectance signal.

- 3) Rather than inverting the image pixel by pixel, the radiometric information of pixels belonging to the same crop field is exploited by assuming limited variability of N , S_z , θ_l , and f_B within the given field, which facilitates iterative model inversion of multiple pixels at the same time. While f_B is initially assumed constant for these high vegetation density pixels ($\text{NDVI} > 0.65$), a pixel-wise disaggregation of f_B occurs in step 4 (Section 4.4).
- 4) An average value of s_1 is initially assumed to represent all pixels considered in the inversion. s_1 is fixed as the average of s_1 derived for low vegetation density pixels ($\text{LAI} < 0.5$) (bare plot within field or nearby sparsely vegetated field) by inversion of ACRM (using Eq. (1)) with default vegetation parameter values (Table 1). Due to the reduced sensitivity of the reflectance observations to background effects at intermediate to high density vegetation coverage (see Section 4.4), consideration of pixel-wise variability in s_1 is less imperative at this stage in the modeling process. In the LUT-based stage of REGFLEC (step 4, Fig. 1), a pixel-wise correction for background effects is implemented (Section 4.4).

Furthermore, a pre-screening technique is used to determine the N , S_z , θ_l and f_B parameter space to be considered in the iterative model

inversion. The pre-screening uses the pre-computed LUTs (Section 4.2) to find a limited number of realistic parameter combinations for the given spectral reflectance dataset, and involves three steps that are performed by looping through each parameter combination (i.e. N_i , $S_{z,i}$, $\theta_{l,i}$ and $f_{B,i}$): a) For all pixels within a given field where $\text{NDVI} > 0.65$, LAI is simulated as a function of observed near-infrared reflectances using the LAI- ρ_{nir} relationship (LUT) specific to the given parameter combination. If the upper or lower LAI bound (see Table 1 for allowable range) is reached for more than 2% of the pixels, the specific parameter combination is regarded as unrealistic and therefore not retained for the iterative inversion runs; b) Similarly spatialized leaf chlorophyll estimates are generated as a function of observed green reflectances, using the LAI estimates in a) to locate the appropriate $C_{\text{ab}}-\rho_{\text{green}}$ LUT relationships, and C_{ab} out of range conditions tested for; and c) If the retrieved LAI and C_{ab} values are within their allowable range (Table 1) for the majority of pixels (98%), the specific parameter combination (i.e. N_i , $S_{z,i}$, $\theta_{l,i}$ and $f_{B,i}$) is only assumed plausible if the average value of f_B calculated using the appropriate f_B -RGVI relationship is within $f_{B,i} \pm 0.025$. This test proved effective as the RGVI exhibits a strong relationship with f_B (Section 4.4).

ACRM is then inverted iteratively by minimizing Eq. (1) for multiple pixels at the same time (i.e. pixels where $\text{NDVI} < 0.65$) with LAI and C_{ab} as free variables for each of the remaining 'realistic' parameter combinations.

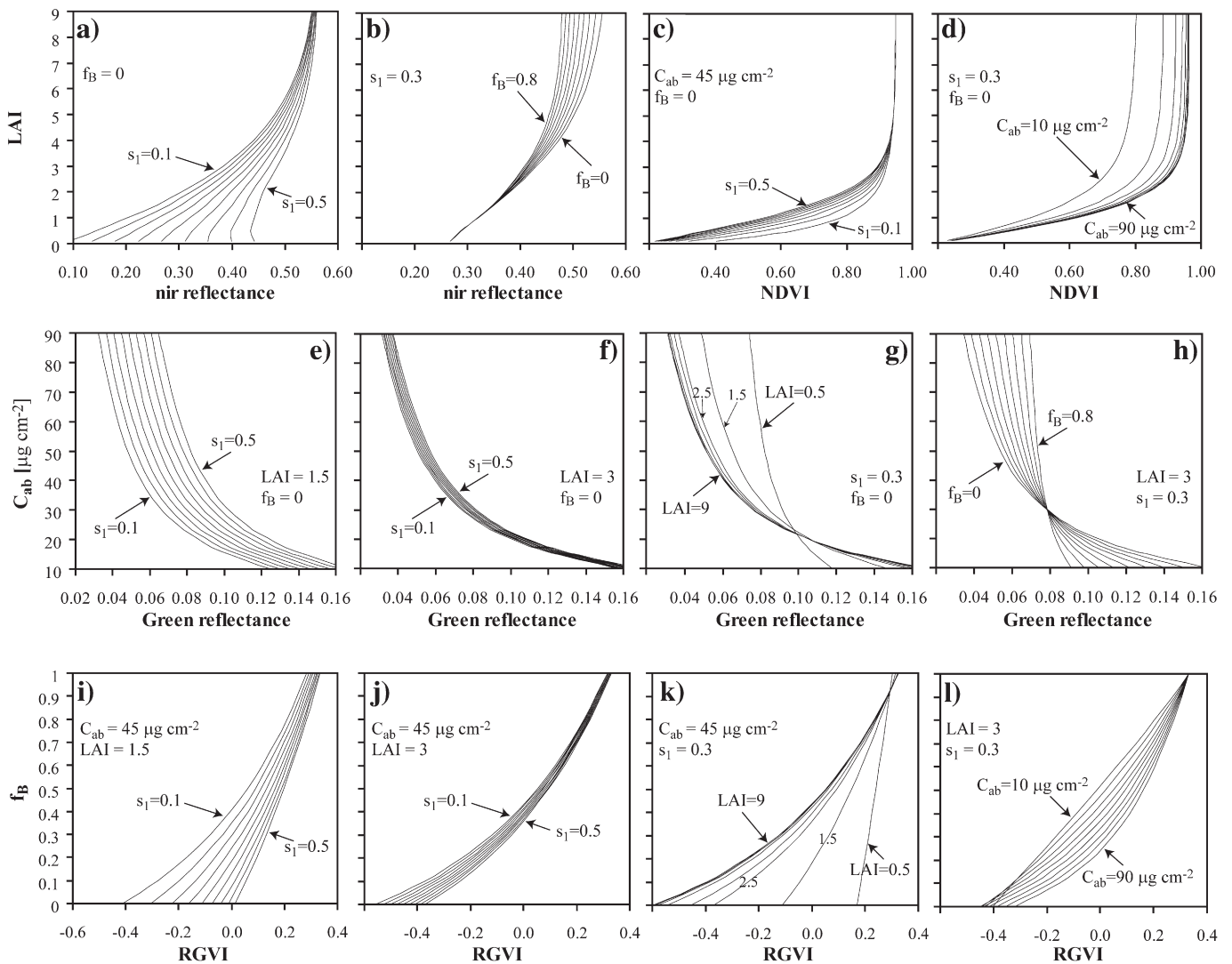


Fig. 2. Spectral reflectance simulated by ACRM model with fixed field specific parameters ($N=1.5$, $S_z=1.0$, $\theta_l=57^\circ$) and view geometries ($\theta_v=20^\circ$, $\theta_s=30^\circ$, $\theta_{\text{raz}}=140^\circ$) and varying LAI, C_{ab} and f_B . Nir and green reflectance, NDVI and RGVI vegetation indices are depicted.



Fig. 3. The OPE3 study area with location of C_{ab} , LAI, and nitrogen treatment field plots. The corn field boundary is indicated by a dashed line. The imagery is a 1 m resolution natural color mosaic acquired by John Deere Agri Services on July 21st.

The set of N , S_z , θ_1 and f_B resulting in the lowest RMS deviation between observed and simulated canopy reflectances is then assumed to apply to the respective field.

ACRM has been optimized, using IDL vector operations, to make the speed of the inversion largely independent of the number of pixels considered. Currently, REGFLEC is arbitrarily set up to use the spectral information content from a minimum of 250 randomly selected pixels or 10% of all pixels within the specific land cover class satisfying the NDVI criteria ($NDVI > 0.65$). Only pixels completely surrounded by pixels of the same field are included to avoid the use of mixed pixels. Additionally, extreme values are avoided due to possible contamination.

4.4. Pixel-wise retrievals of LAI and C_{ab} (step 4)

With the field-specific determination of N , S_z and θ_1 completed pixel-wise estimates of LAI and C_{ab} can be generated for the entire field using the pre-computed look-up tables described in Section 4.2. The LAI- ρ_{nir} LUT is reduced from a multi-dimensional array of 6 dependent variables

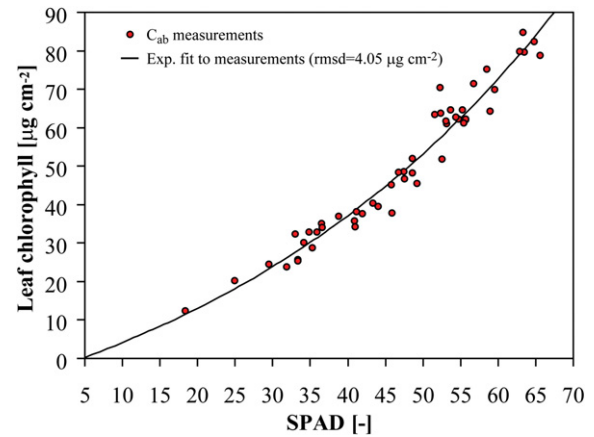


Fig. 4. The derived empirical SPAD- C_{ab} relationship based on leaf samples collected during the 2005 and 2007 experimental campaigns.

to only 2 dependent variables (f_B and s_1) while the C_{ab} - ρ_{green} LUT is reduced to a 3 dimensional array (LAI, f_B and s_1 being the dependent variables) (Section 4.2).

Fig. 2 illustrates a sample of model generated spectral reflectance relationships, stored in the pre-computed LUTs (Section 4.2) for a theoretical field ($N=1.5$, $S_z=1.0$, $\theta_1=57^\circ$, $\theta_v=20^\circ$, $\theta_s=30^\circ$, $\theta_{raz}=140^\circ$), demonstrating the sensitivity of LAI, C_{ab} and f_B to various reflectance and vegetation index values. Fig. 2a illustrates the strong sensitivity of LAI- ρ_{nir} relationships to variations in soil reflectance (s_1) even for dense vegetation as a result of high canopy penetration capabilities of ρ_{nir} . The influence of f_B on LAI estimation is only significant for fairly high vegetation densities (Fig. 2b). While soil reflectance contributes to the green reflectance signal at low vegetation densities (Fig. 2e), the inability of radiometers operating in the green spectrum to sense through a leaf layer (Lillesaeter, 1982) minimizes the effect of the background signal at

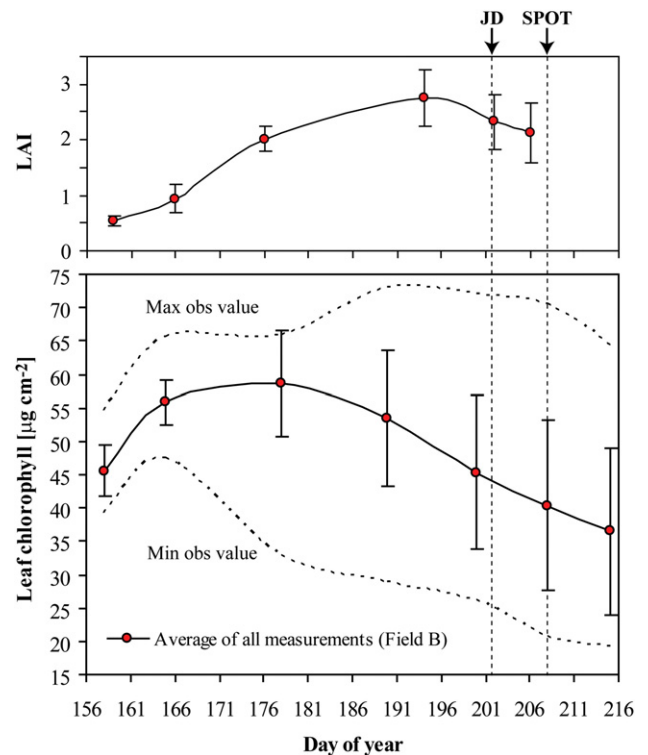


Fig. 5. Timeseries of LAI and leaf chlorophyll as measured in field B (Fig. 3). The bars represent the standard deviation of all the measurements made within field B. The maximum and minimum measured leaf chlorophyll values are also shown. The arrows indicate the time of John Deere (JD) and SPOT image acquisitions.

intermediate vegetation densities (Fig. 2f). Moreover C_{ab} – ρ_{green} relationships are only affected by LAI variations at low to intermediate vegetation densities (Fig. 2g). As expected, the sensitivity of ρ_{green} to changing leaf chlorophyll content is reduced with increasing amount of senescent leaf material (Fig. 2h). The low sensitivity to the background reflectance signal and LAI variations at intermediate to high vegetation densities are shared by the f_B –RGVI relationships (Fig. 2i–k).

Preliminary estimates of LAI and C_{ab} are generated for every pixel within the specific land cover class from the LAI– ρ_{nir} and C_{ab} – ρ_{green} LUTs using the land cover averaged values of f_B and s_1 (derived in the iterative inversion step), as LUT entries. LAI is estimated first, then the C_{ab} – ρ_{green} relationship appropriate to the LAI of each pixel is applied to estimate C_{ab} (Fig. 2g). The preliminary LAI and C_{ab} estimates are then used to disaggregate f_B spatially from relationships stored in the f_B –RGVI LUT (Fig. 2i–l).

It is evident from Fig. 2 that soil background effects may confound the canopy signal when employing single spectral band relationships for biophysical parameter estimations. While soil background influences can also be detected in the LAI–NDVI relationships (Fig. 2c), the vegetation index normalization reduces the dependency on s_1 significantly. On the other hand, the translation of spectral reflectance data into a vegetation index often reduces the sensitivity to the parameter of interest. For instance, the NDVI signal saturates at intermediate vegetation densities (Fig. 2c and d) whereas ρ_{nir} remains responsive to changing leaf biomass up to LAI ~6 (Fig. 2a). At low to intermediate vegetation cover, a mismatch in LAI estimated using ρ_{nir} and NDVI, respectively is most likely due to an

erroneous s_1 value (Fig. 2a and c). The LAI divergence between the two estimates can be significant as the NDVI based LAI estimate will only vary by a maximum of approximately ± 0.5 while LAI discrepancies of up to 5 (in addition to large negative LAI values) are likely for the ρ_{nir} based estimates as a result of inaccurate s_1 data (Fig. 2a and c). As the two LAI estimates should coincide if the background effect is properly accounted for, a pixel-wise correction for background effects was facilitated by adjusting s_1 to cause a match between LAI values generated as a function of ρ_{nir} and NDVI, respectively. The resulting map of s_1 is then used to update LAI, C_{ab} and f_B using the respective LUTs.

5. Field experiment

The REGFLEC tool was applied to remotely sensed reflectance observations of a corn (*Zea mays* L.) crop field located within the USDA-ARS Beltsville Agricultural Research Center, Maryland (39.02° N, 76.85° W). The study site is associated with the Optimizing Production Inputs for Economic and Environmental Enhancement (OPE3) program, and consists of four surface hydrologically bounded sub-watersheds, about 4 ha each, which feed a wooded riparian wetland and first-order stream. The watersheds were formed from sandy fluvial deposits and have a varying slope ranging from 1% to 4% (for further details see <http://hydrolab.arsusda.gov/o3e3/>).

This study focuses on data collected during the 2007 growing season. Leaf and canopy data were collected from early June, shortly after corn emergence, to the beginning of August. The average daily mean

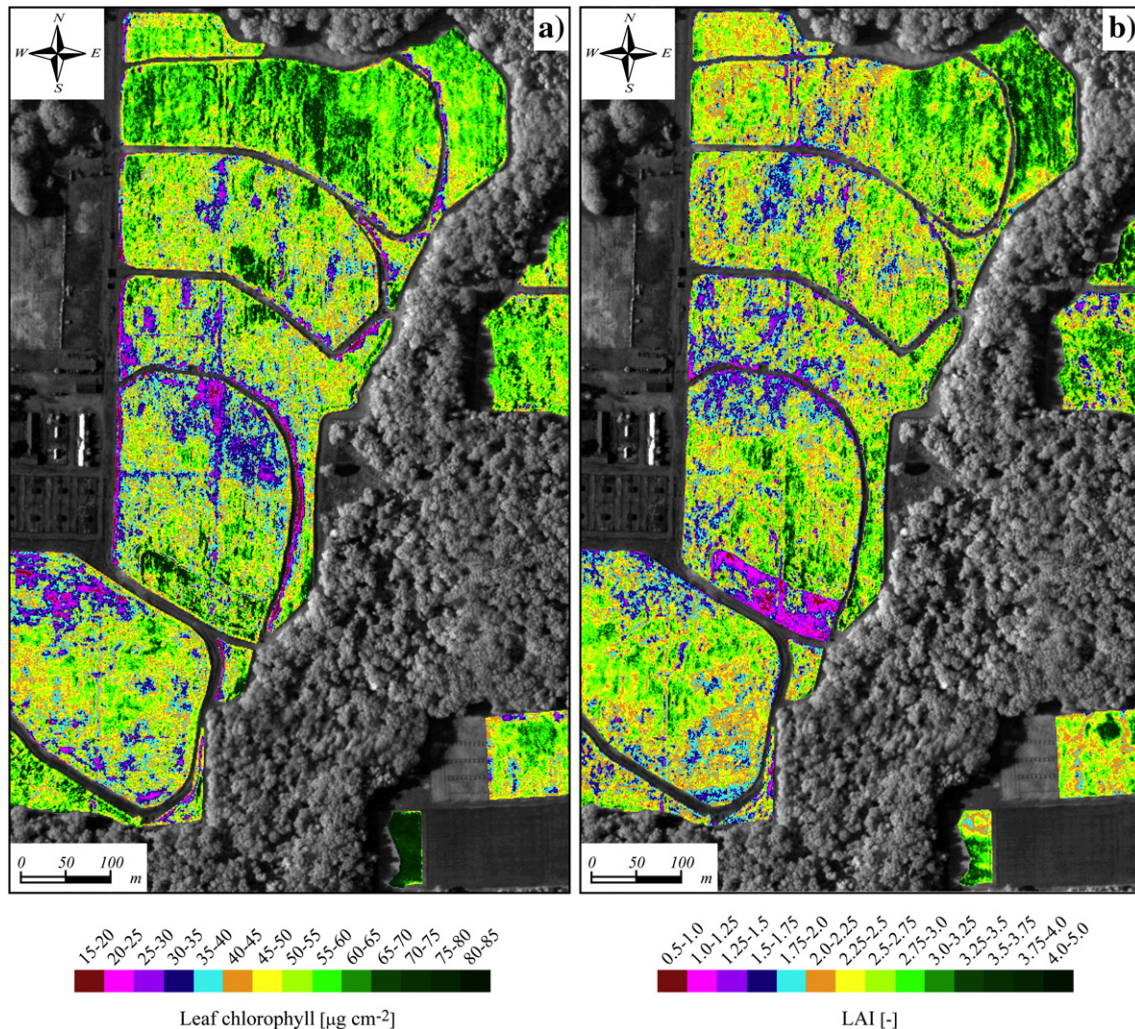


Fig. 6. REGFLEC derived maps of leaf chlorophyll (a) and LAI (b) for the corn field using 1 m resolution aircraft data as input. The background is the near-infrared 1 m resolution image.

temperature for June and July was 22.3° and 24.2°, respectively and the precipitation was well below average from around mid-June. This resulted in significant crop drought stress in the latter part of the study period.

5.1. Biophysical measurements

Measurements of LAI and leaf chlorophyll were collected at weekly intervals throughout the study period at 25 field plots each having a size of approximately 2 m × 2 m. Each plot was accurately geolocated using a differential global positioning system. Supplementary data were collected on August 1st at 6 larger plots (15 m × 15 m) (Fig. 3) that were geolocated using a handheld Global Positioning System (GPS) unit (accuracy ≈ 4 m). Additionally, 24 nitrogen treatment plots with a size of 9 × 26 m were sampled (Fig. 3). Ammonium nitrate was applied shortly after planting and on June 6th to supply 0%, 50%, 100%, and 200% of the recommended rate of 140 kg N/ha and to establish a range of leaf chlorophyll levels.

LAI was estimated non-destructively using a LAI-2000 instrument (LiCor, USA).¹ The LAI measurements were made shortly after sunrise, shortly before sunset or during overcast conditions using a 270° view cap to prevent interference caused by the operator's presence. Four readings were made along diagonal transects between the rows as suggested in the LAI-2000 manual for row crops, and repeated once (8 below canopy readings in total). We have found that this measurement protocol results in LAI values that are in good agreement with the 'true' LAI (i.e. from destructive leaf sampling). In the 2 × 2 m plots, the average of two LAI-2000 measurements (2 × 8 readings) was used whereas the 15 × 15 m plots were represented as the average of 5 separate measurements (5 × 8 readings).

Leaf chlorophyll content was measured non-destructively with a portable SPAD-502 Chlorophyll meter (Spectrum Technologies, Inc.).¹ This instrument measures leaf transmittance at two wavelengths: red (650 nm) where light absorbance by chlorophyll is efficient and near-infrared (940 nm) where absorbance by chlorophyll is insignificant. The SPAD-502 meter calculates a non-dimensional SPAD value (0–99) according to

$$\text{SPAD} = k \cdot \log 10 \frac{T_{940}}{T_{650}} \quad (4)$$

where T is the transmittance and k is a calibration coefficient determined by the manufacturer (Uddling et al., 2007). The claimed accuracy of the meter output is ±1 SPAD unit.

Six separate measurements with the SPAD-502 were made on each leaf to properly describe the variability across the leaf. In each of the 2 m × 2 m plots, the average of 18 × 6 SPAD readings was used, and in the larger plots, the average of approximately 50 × 6 SPAD readings was used. During the measurements the sensor head was shaded to avoid direct sunlight from reaching the instrument. In stands with a mix of green and senescent leaves, only the green leaves were measured.

In order to convert the unit-less SPAD values into absolute measures of leaf chlorophyll, a relationship between leaf chlorophyll content and SPAD values must be initially determined. For this purpose leaf chlorophyll was measured spectrophotometrically in the laboratory after extraction of chlorophyll with *N*,dimethyl sulfoxide (DMSO) (Wellburn, 1994). Since a wide range of leaf chlorophyll contents is required for establishing a reliable empirical fit, the derived SPAD– C_{ab} relationship (Fig. 4) is based on leaf samples collected during the 2005 and 2007 experimental campaigns. The relationship used to convert the SPAD-502 measurements into leaf chlorophyll content ($\mu\text{g cm}^{-2}$) reads

$$C_{ab} = 33.9042 \cdot \exp(\text{SPAD} \cdot 0.0196) - 37.1544 \quad (\text{RMSD} = 4.1 \mu\text{g cm}^{-2}) \quad (5)$$

The exponential fit is in agreement with other studies that have reported deviations from linearity in the high and low SPAD range (Markwell et al., 1995; Richardson et al., 2002; Uddling et al., 2007).

5.2. SPOT reflectance observations

Radiance data in the green (500–590 nm), red (610–680 nm) and near-infrared (780–890 nm) wavebands were acquired by the SPOT-5 High Resolution Geometric imaging instrument (HRG-2) on July 27th. The SPOT-5 radiances were obtained in 10 m resolution at 12:13 p.m. local time for a 30 km × 30 km image swath. The level 2A SPOT data are rectified to match a standard cartographic projection (UTM WGS84) using cubic convolution resampling by default. The location accuracy is better than 30 m (www.spot.com). However, convolution resampling is inappropriate for research applications like this since the convolution averages neighboring pixels to provide a smoother appearance thereby losing the original radiometric signal of the image pixels. To preserve the information content of the individual pixels, image-to-image rectification was applied to the level 1A product (no geometric corrections performed) using the geolocated level 2A product as reference and a nearest neighbor resampling technique. The geolocation accuracy was further improved by matching the SPOT scene with the airborne imagery described in Section 5.3.

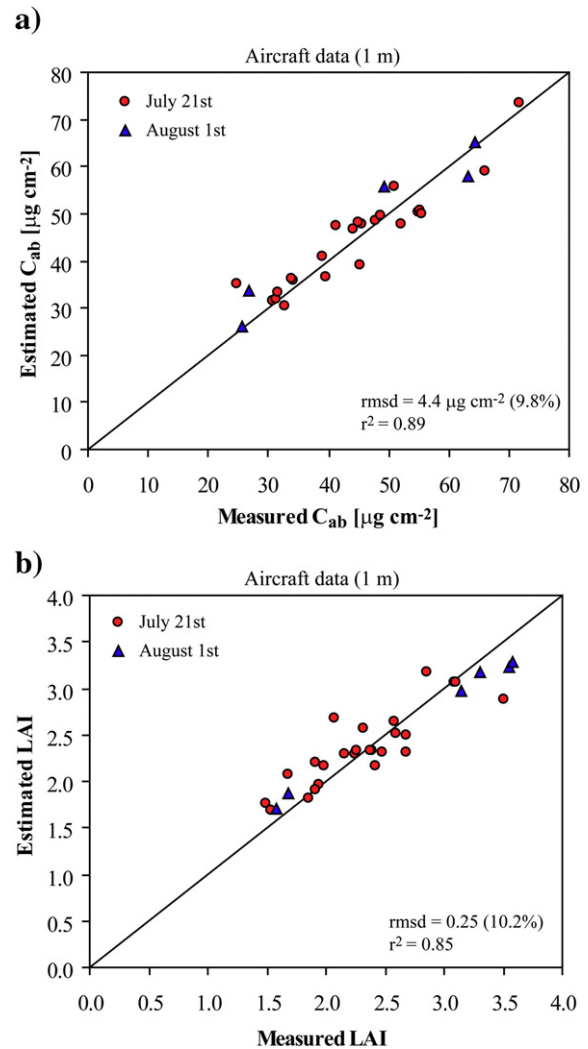


Fig. 7. Validation of 1 m resolution leaf chlorophyll (a) and LAI (b) estimates using field measurements collected within 2 × 2 m (circles) and 15 × 15 m (triangles) field plots. The r^2 value and the absolute and relative RMS deviation between estimates and measurements are listed. The thick line is the 1:1 line.

¹ Trade names are included for the benefit of the reader and do not imply an endorsement of or a preference for the product listed by the U.S. Department of Agriculture.

The geometrically and radiometrically corrected radiances were input to the coupled 6SV1-PROSPECT-ACRM (REGFLEC) radiative transfer scheme (Section 4). The values used for the additional 6SV1 input parameters are listed in Table 1. The level 2.0 Aerosol Robotic Network (AERONET) aerosol optical depth (τ_{550}) and total precipitable water (TPW) data from the nearby NASA GSFC site were used (Holben et al., 1998). Atmospheric ozone measurements (O_3) were extracted from the Atmospheric InfraRed Sounder (AIRS) level 2 standard retrieval product that reports the atmospheric properties at a spatial resolution of $45 \text{ km} \times 45 \text{ km}$. If local sun photometer measurements are unavailable, τ_{550} data from the Terra or Aqua MODIS aerosol product (MOD/MYD04) are a good alternative. Validation studies have suggested the expected error over vegetated land surfaces to be represented by $\pm(0.05 + 0.15\tau_{550})$ (Remer et al., 2005; Vermote et al., 2002; Houborg et al., 2007b). The AIRS TPW product has been validated with an uncertainty estimate of 5–20% (<http://disc.sci.gsfc.nasa.gov/AIRS/documentation.shtml>), and may be preferred over localized radiosonde observations that are only available at widely separated sites and therefore may not be representative of the atmospheric conditions of the area to be mapped. For the present study region, the MODIS derived τ_{550} (0.2) and the AIRS derived TPW (3.71) are in good agreement with the sun photometer measurements (Table 1).

5.3. Aerial imagery

An aerial digital image of the study region was acquired by John Deere Agri Services on July 21st. The sensor system consists of four 12-bit digital cameras with a 1600 by 1200 pixel charge coupled device (CCD). Digital image data in the green (510–580 nm), red (610–690 nm) and near-infrared (800–900 nm) wavelength regions were provided at a spatial resolution of 1 m and georegistered with a horizontal accuracy of approximately $\pm 1 \text{ m}$. Unfortunately, radiometric calibration coefficients for the conversion of digital counts to radiances are not provided with the product. Instead the conversion

to surface reflectance was facilitated by matching the digital counts with the 6SV1 atmospherically corrected SPOT surface reflectances for a set of carefully selected areas in the study region. This approach is assumed viable since the SPOT and John Deere (JD) acquisitions were only 6 days apart, and the selected areas experienced a minimal change in LAI and leaf chlorophyll between the acquisitions (as determined by field measurements). Band specific (green, red and near-infrared) linear regression of the digital counts in the JD image and the SPOT surface reflectances for the selected areas resulted in correlations of determinations (r^2) close to unity (0.98–0.995). The regression equations were then used to convert all digital counts to reflectance units.

6. Results

Fig. 5 illustrates the temporal progression of leaf chlorophyll and LAI, measured in field B (Fig. 3), from approximately 3 weeks after leaf emergence (day of year (DOY) 134) through corn tasseling and silking (DOY 193) and a stage of leaf senescence. The average C_{ab} of field B initially increased from $\sim 45 \mu\text{g cm}^{-2}$ to a peak value of $\sim 57 \mu\text{g cm}^{-2}$ at around DOY 180. The LAI most likely peaked shortly hereafter but cannot be verified due to the gap in measurements (Fig. 5). The onset of drought conditions caused the average C_{ab} to decrease continuously reaching a minimum of $\sim 35 \mu\text{g cm}^{-2}$ and an overall drop in LAI was also observed during this time period. However, the degree of plant stress imposed by extreme environmental conditions throughout much of July and the beginning of August varied widely across field B, as illustrated by the high standard deviations and observed C_{ab} ranges of approximately 20–70 $\mu\text{g cm}^{-2}$ during peak stress conditions (Fig. 5). Both image acquisitions occurred during a late stage of corn maturity where the corn in many places was significantly stressed and in an advanced stage of leaf senescence (Fig. 5). These conditions allow for model validation over a wide range in leaf chlorophyll content and for the complex case of green leaf material intermixed with senescent material.

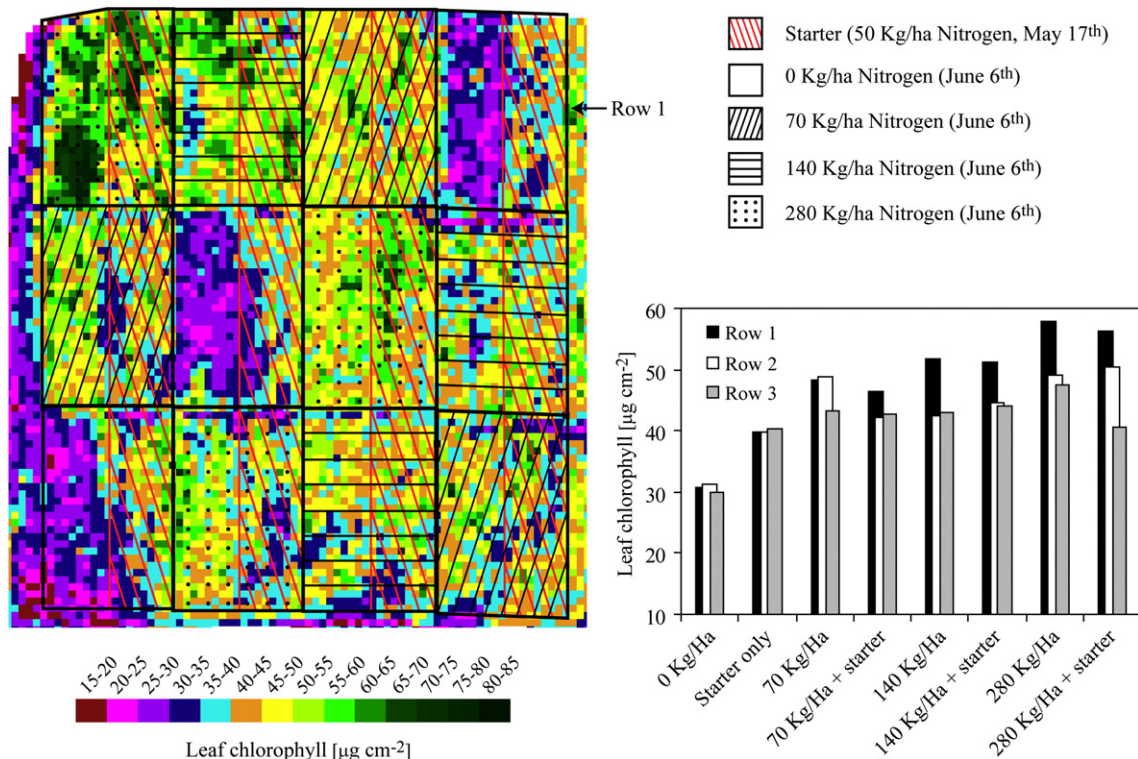


Fig. 8. A blow up of the 1 m resolution leaf chlorophyll map for the area containing the nitrogen treatment plots (see Fig. 3). Nitrogen was applied on May 17th and June 6th according to the nomenclature. The associated graph displays the average C_{ab} within each of the 24 treatment plots sorted as a function of the nitrogen application rate.

6.1. LAI and leaf chlorophyll estimates (1 m resolution)

Fig. 6a and b illustrates the results of running REGFLEC with input of 1 m resolution spectral aircraft data. For these model runs the leaf inclination angle was fixed to 60° , which was the average of the field measurements obtained using the LAI-2000. The initial estimate of the soil background signal (s_1) (Section 4.3) was derived using reflectance observations from a sparsely vegetated area in vicinity of the study area (the bright area in the lower right corner of the study area – Fig. 3). The pixel-wise estimates of C_{ab} (Fig. 6a) were generated using a family of C_{ab} – ρ_{green} relationships, each being a function of corn specific characteristics (N , S_z , θ_l), soil background reflectance signal (s_1), fraction of senescent material (f_B) and LAI (see Section 4.4). The iterative inversion (Section 4.3) resulted in a value of 1.7 for the leaf mesophyll structure parameter, N , and a value of 1.0 for the Markov clumping parameter, S_z . C_{ab} shows significant spatial heterogeneity on this date, varying from 15–85 $\mu\text{g cm}^{-2}$. The northerly part of the field (field A) appears to be the least stressed with most parts of the field having C_{ab} values greater than 50 $\mu\text{g cm}^{-2}$. High C_{ab} values tend to coincide with high amounts of leaf biomass while significantly stressed areas generally have lower values of LAI (Fig. 6b). However, LAI is here the total LAI and thus includes green as well as senescent plant material. The LAI map was generated using LAI– ρ_{nir} relationships specific to the corn field (i.e. $N=1.7$, $S_z=1.0$, $\theta_l=60^\circ$) reflecting pixel-wise variations in s_1 and f_B (Section 4.4).

Areas with high values of LAI and C_{ab} generally correspond very well with higher producing regions within the field as identified by

Gish et al. (2001). Gish et al. (2001) found a marked degree of similarity in the spatial pattern of the higher producing regions for two drought years and demonstrated that high yielding areas were closely related with areas over subsurface flow pathways.

The accuracies of the C_{ab} and LAI retrievals were evaluated by comparison with data collected at the field plots depicted on Fig. 3. The comparisons use the average value of a 2×2 and 15×15 pixel block around the center of the small and large field plots, respectively. C_{ab} data collected at the small field plots on July 19th and July 27th and LAI data collected at the same plots on July 13th and July 25th were linearly interpolated to be concurrent with the aircraft overpass day (July 21st). The August 1st data refer to samplings at the larger (15×15 m) plots (Fig. 1). The model shows excellent capability in reproducing the pattern in measured leaf chlorophyll (Fig. 7a) and LAI (Fig. 7b) with an r^2 of 0.89 and 0.85, respectively and a relative RMS deviation of 9.8% and 10.2, respectively.

Leaf chlorophyll is highly correlated with leaf nitrogen, as much of leaf nitrogen is incorporated in chlorophyll (Filella et al., 1995). A closer look at the variability in C_{ab} at the OPE3 nitrogen treatment plots (see Fig. 3) is given in Fig. 8. Nitrogen was applied to each rectangular area with rates of either 0 or 50 kg/ha on May 17th and 0, 70, 140 or 280 kg/ha on June 6th. The estimated leaf chlorophyll values generally discriminate the various nitrogen treatments well and an increase in leaf chlorophyll levels with increasing nitrogen rates can be clearly identified especially for the treatment plots in row 1 (Fig. 8). The plots that received no nitrogen coincide with stressed areas

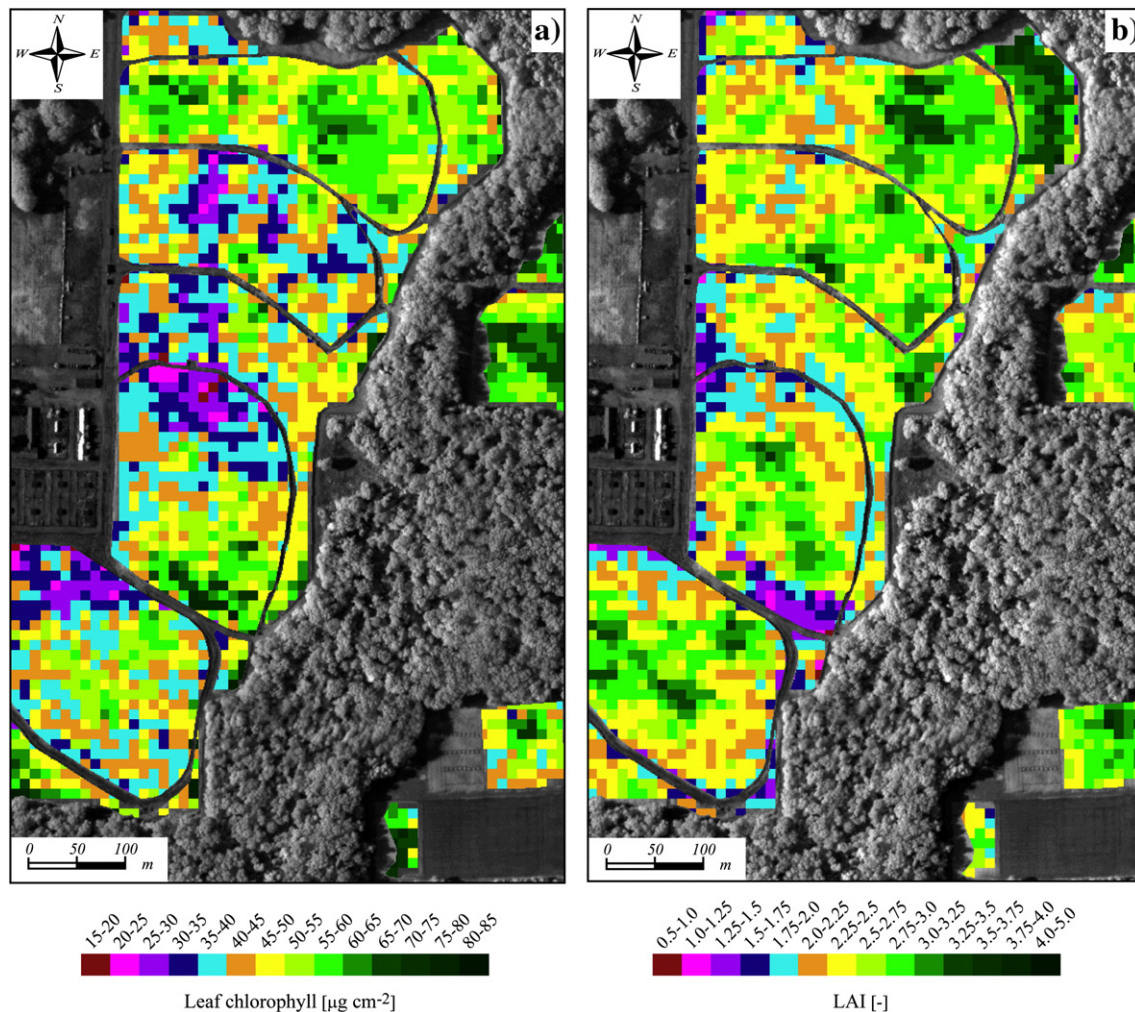


Fig. 9. REGFLEC derived maps of leaf chlorophyll (a) and LAI (b) using 10 m resolution SPOT-5 data as input. The background is the 1 m resolution near-infrared image.

characterized by modeled C_{ab} values on the order of $20\text{--}30\ \mu\text{g cm}^{-2}$. In contrast, an average leaf chlorophyll content of $59\ \mu\text{g cm}^{-2}$ was modeled for the plot in the upper left corner, which received maximum rates of nitrogen application (Fig. 8). A perfect correspondence between C_{ab} and the nitrogen application rates is not observed for all plots, which is expected in light of the additional plant stress that may have been imposed by the extreme environmental conditions that occurred after the last nitrogen treatment.

6.2. LAI and leaf chlorophyll estimates (10 m resolution)

Fig. 9a and b illustrates REGFLEC outputs of LAI and C_{ab} derived using 10 m resolution SPOT data. The corn-specific iterative inversion results of N (1.73) and S_z (0.98) are comparable to those retrieved using the aircraft data. While much of the fine-scale variability in the parameters is lost at this resolution, the overall intra-field pattern in LAI and C_{ab} is well-established.

Comparing C_{ab} measurements collected at the day of the SPOT acquisition (July 27th) and 5 days later (August 1st) with estimates extracted from the $10\times 10\text{ m}$ pixel closest to each field plot results in a good agreement with a relative RMSD of 17.1% (Fig. 10a). The fit is excellent for the large validation plots that were specifically designed

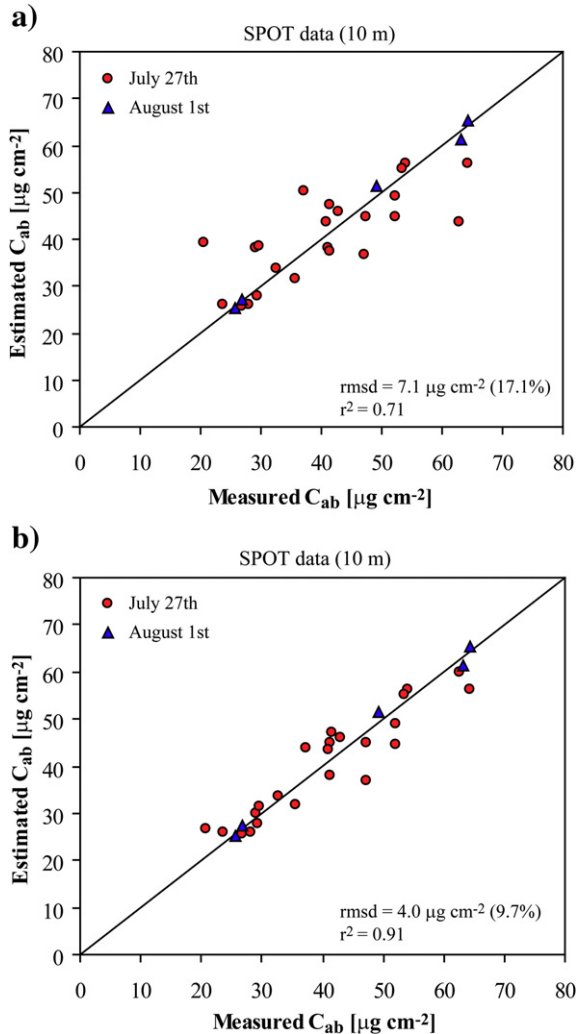


Fig. 10. Validation of 10 m resolution leaf chlorophyll estimates using the pixel value closest to each field plot (a) or the best matching pixel value for field plots located on the boundary of two neighboring pixels (b). The validation data were collected at $2\times 2\text{ m}$ (circles) and $15\times 15\text{ m}$ (triangles) field plots. The r^2 value and the absolute and relative RMS deviation between estimates and measurements are listed. The thick line is the 1:1 line.

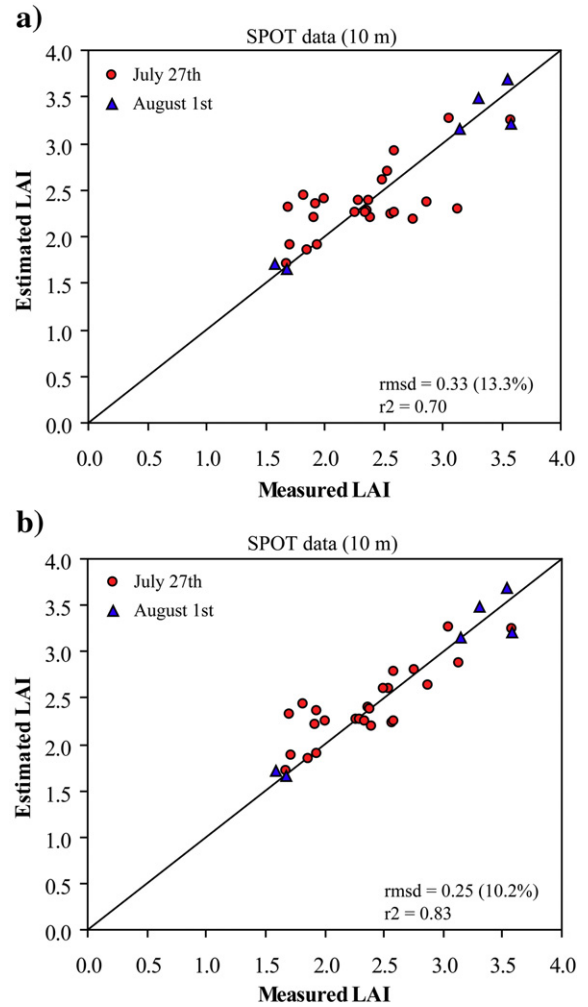


Fig. 11. Validation of 10 m resolution LAI estimates using the pixel value closest to each field plot (a) or the best matching pixel value for field plots located on the boundary of two neighboring pixels (b). The validation data were collected at $2\times 2\text{ m}$ (circles) and $15\times 15\text{ m}$ (triangles) field plots. The r^2 value and the absolute and relative RMS deviation between estimates and measurements are listed. The thick line is the 1:1 line.

for validating the SPOT retrievals. The greater discrepancies observed for some of the $2\times 2\text{ m}$ field plots are expected considering the large sub-pixel variability in C_{ab} at the 10 m scale (Fig. 6a). Fine-scale C_{ab} variability and small registration errors could easily cause the nearest pixel value to be non-representative of the conditions at these field plots. Fig. 10b illustrates the C_{ab} validation results when the best matching pixel values are used for field plots located on the boundary of two neighboring pixels. The result is a significantly improved fit characterized by an r^2 of 0.91 and a relative RMS deviation of 9.7%.

The LAI validation results are shown in Fig. 11a and b. While LAI appears to be less affected by the scale difference, the use of best matching pixel values rather than the nearest pixel values (only for field plots located on the boundary of two neighboring pixels), causes an increase in accuracy from a relative RMS deviation of 13.3% to 10.2% (Fig. 11). For these comparisons, LAI measurements collected at the small field plots on July 25th and July 31st were linearly interpolated to be concurrent with the SPOT overpass day (July 27th).

6.3. Canopy fraction of senescent material

An average value of f_B , representative of 'dense' vegetation ($\text{NDVI} > 0.65$) pixel elements, was derived during the REGFLEC iterative inversion mode (Section 4.3). A spatial disaggregation of f_B , for every pixel within

the field boundary was facilitated by applying corn-specific f_B -RGVI relationships (Section 4.4). The generated 1 m resolution f_B map (Fig. 12) indicates an advanced stage of canopy senescence in many parts of the field with an overall average f_B of approximately 0.35. The spatial pattern follows quite closely the distribution of leaf chlorophyll content (Fig. 6a) with areas of high C_{ab} corresponding to low amounts of senescent leaf material. Photographs of the corn field from a number of selected plots illustrate quite variable amounts of senescent plant material and demonstrate ability of the model for the delineation of horizontal gradients in f_B (Fig. 12). The photographs also illustrate the diversity within the site in terms of plant density and degrees of plant stress.

6.4. Model parameter sensitivity

6.4.1. Leaf inclination angle

The above results were all generated using prior information to fix the leaf inclination angle (set to 60° based on field measurements). θ_1 is an influential factor in visible and near-infrared reflectance spectra (Bacour et al., 2002b) but is difficult to retrieve accurately from model inversion since LAI and θ_1 counterbalance each other (Baret & Guyot, 1991). This may cause different sets of LAI and θ_1 to correspond to almost identical spectral signatures. Atzberger (2004) demonstrated that adjacent pixels belonging to the same crop field contain supplementary spectral information, which helps reduce confounding effects between

LAI and θ_1 . Intra-field radiometric information content is also exploited in REGFLEC and there is an option to include θ_1 as a free variable in the iterative inverse mode (Section 4.3). Invoking the θ_1 free mode for the 1 m resolution aircraft data resulted in the following values for the class-specific parameters: $N=1.4$, $S_z=0.89$ and $\theta_1=56^\circ$. The value of 1.4 for the leaf mesophyll structure parameter is in agreement with the value ($N=1.41$) derived in Haboudane et al. (2004) by inverting the PROSPECT model on corn reflectance and transmittance spectra measured in the laboratory, and the value used for corn plants by Jacquemoud et al. (2000). The retrieved value of S_z (0.89) is at the high end of clumping values reported by Demarez et al. (2008) using hemispherical photographs but is consistent with clumping factors derived for a mature corn stand using techniques described in Li et al. (2005) and Anderson et al. (2005), which account for effects of non-random leaf area distribution characteristic of row crops. Verification of the LAI and C_{ab} measurements against these new maps resulted in retrieval accuracies comparable to those retrieved using prior information to fix θ_1 (Table 2).

6.4.2. Soil background effects

Background reflectance can be a significant contributor to the canopy reflectance signal (Daughtry et al., 2000; Haboudane et al., 2004) and care should be utilized to avoid confounding effects between vegetation parameters (e.g. f_B , C_{ab} and LAI) and the soil parameter, s_1 , especially at low vegetation coverage. A novel soil correction scheme was

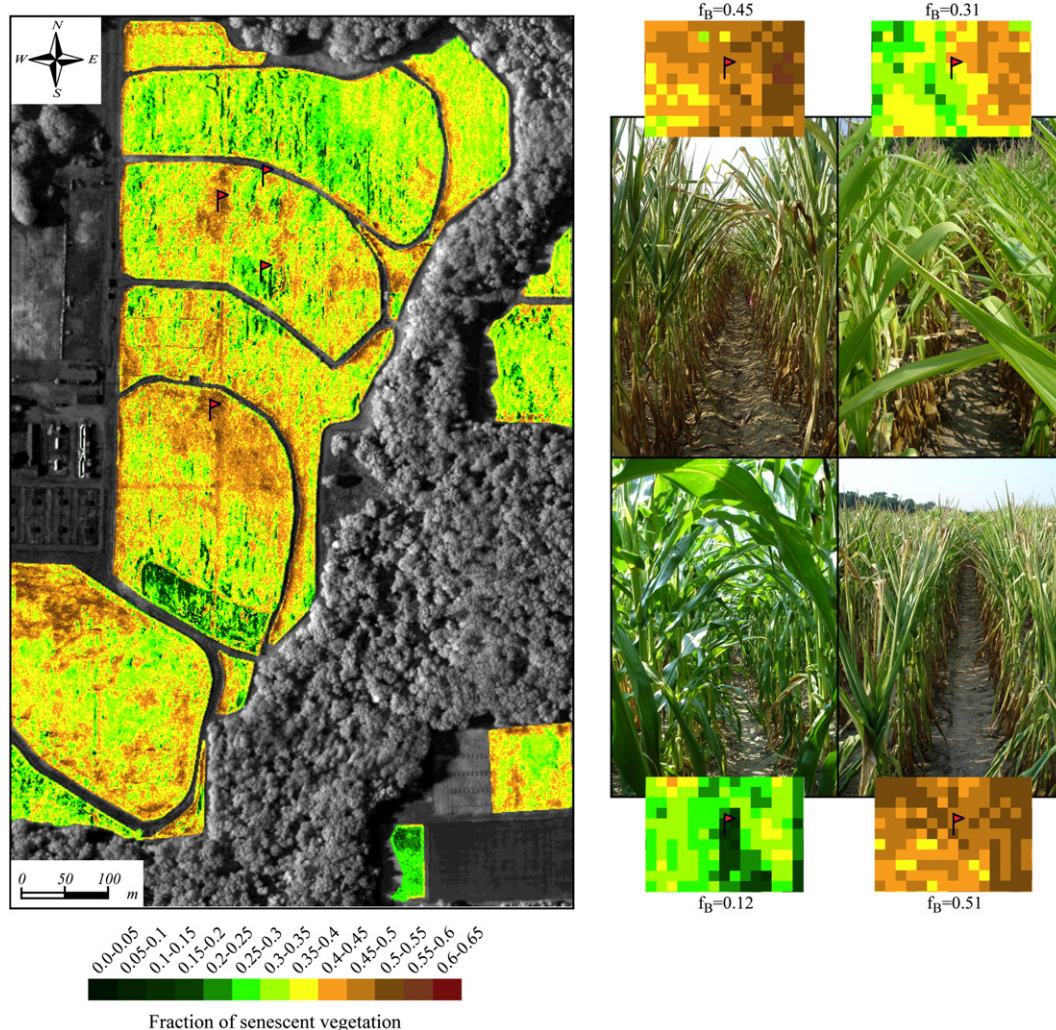


Fig. 12. REGFLEC derived map of 1 m resolution canopy fraction of senescent vegetation (f_B). Photographs of the corn plant from 4 selected plots (red flags) are also shown along with a zoomed view of the derived f_B values around the area where the photographs were taken. (For interpretation of the references to color in this figure legend, the reader is referred to the web version of this article.)

Table 2

Validation statistics of LAI and C_{ab} as a result of running REGFLEC with θ_1 fixed (using the value derived from LAI-2000 measurements) and free (iterative inversion estimate in parentheses)

Aerial imagery	n		Mean		RMSD		RRMSD [%]		r^2		Bias [%]	
	LAI	C_{ab}	LAI	C_{ab}	LAI	C_{ab}	LAI	C_{ab}	LAI	C_{ab}	LAI	C_{ab}
θ_1 fixed (60°)	31	28	2.5	45.1	0.25	4.4	10.1	9.75	0.85	0.89	0.3	1.2
θ_1 free (56°)	31	28	2.4	44.8	0.23	5.2	9.5	11.6	0.89	0.87	-2.5	5.2

The root-mean-square deviation (RMSD), relative RMSD (RRMSD) and Bias is defined below. r^2 is the determination coefficient and n the number of measurements.

$$\text{RMSD} = \left[\frac{\sum_{i=1}^n (P_i - O_i)^2 / n}{\sum_{i=1}^n (O_i)^2 / n} \right]^{1/2}, \text{RRMSD} = \frac{\text{RMSD}}{\sum_{i=1}^n (O_i) / n} \cdot 100\%, \text{Bias} = \frac{\sum_{i=1}^n (P_i - O_i)}{n}.$$

implemented to minimize the influence of within-field variability in background reflectance on the estimation accuracy of the biophysical parameter retrievals. An approximate estimate of s_1 , derived by model inversion using reflectance spectra from a nearby soil field or partially vegetated field, is required initially as input. The initial s_1 estimate is then adjusted iteratively during the inverse mode to provide a best fit between modeled and measured reflectance spectra (Section 4.3). Finally, a pixel-wise correction for background effects is facilitated by adjusting s_1 to produce a match between LAI values generated as a function of ρ_{nir} and NDVI, respectively (Section 4.4). Ignoring intra-field variations in soil reflectance (i.e. fixing s_1 with the initial estimate throughout the corn field) has a significant impact on the spatial estimates of LAI and C_{ab} (Table 3). The LAI estimates decrease uniformly throughout the field (Bias=-9%) (Table 3). The effect on C_{ab} varies significantly from pixel to pixel as illustrated by a low inter-correlation ($r^2=0.56$) and high RMS deviation between the two maps of C_{ab} generated with the soil background correction turned on and off, respectively (Table 3). Additionally, the upper and lower C_{ab} bounds are reached for 5% of the pixels (=11,400 pixels) compared to only 0.5% when variations in background reflectance are considered. More importantly, the C_{ab} predictability is seen to deteriorate from a relative RMS deviation of 10% and r^2 of 0.89 to a relative RMS deviation of 25.8% and r^2 of 0.21 (Table 3).

6.4.3. Atmospheric effects

Remotely sensed reflectance observations are not free of errors; the transformation of sensor digital counts into surface reflectance values will inevitable be associated with some degree of uncertainty (Combal et al., 2002a). The atmospheric correction is probably the most critical element. The conversion of radiance data into surface reflectance in the visible and near-infrared spectrum is most sensitive to the aerosol optical depth (τ) and type of aerosol model (Vermeulen & Vermeulen, 1999). Table 4 demonstrates the sensitivity of the key model output (LAI and C_{ab}) to uncertainties associated with τ_{550} and type of aerosol model. The expected error of the operational MOD/MYD04 aerosol product ($\pm(0.05+0.15\tau)$) was assumed in the sensitivity runs to reflect opera-

Table 3

The impact on the 1 m resolution spatial estimates of LAI and C_{ab} as a result of ignoring intra-field variations in soil reflectance

Aircraft data	n	Mean		r^2		RMSD		RRMSD [%]		Bias [%]	
		LAI	C_{ab}	LAI	C_{ab}	LAI	C_{ab}	LAI	C_{ab}	LAI	C_{ab}
Entire scene	212,830	2.34	49.1	0.96	0.56	0.25	10.4	10.7	21.2	-9.1	1.0
Validation sites	31	2.42	44.6	0.88	0.21	0.37	11.5	15.3	25.8	-12.7	5.2

The statistics (see Table 2 for definition of statistical descriptors) describe the agreement between LAI and C_{ab} spatial datasets (all pixels, $n=212,830$) generated by fixing s_1 with the initial estimate throughout the corn field and by correcting for pixel-wise variations in s_1 , respectively. A negative Bias indicates that dataset values not corrected for soil background effects underestimates dataset values corrected for background effects. The agreement of the uncorrected dataset with the ground truth data ($n=31$) is also shown. The LAI and C_{ab} data were generated using the input data listed in Table 1 and a leaf inclination angle of 60°.

Table 4

Sensitivity of 10 m resolution REGFLEC estimates of LAI and C_{ab} to uncertainties in 6SV1 critical input parameters (aerosol optical depth and type of aerosol model)

SPOT data	n	Mean		r^2		RMSD		RRMSD [%]		Bias [%]	
		LAI	C_{ab}	LAI	C_{ab}	LAI	C_{ab}	LAI	C_{ab}	LAI	C_{ab}
$\tau_{550}=0.31$	2420	2.59	44.9	0.92	0.84	0.20	4.9	8.0	10.6	3.5	-3.8
$\tau_{550}=0.15$	2420	2.37	47.8	0.91	0.93	0.17	3.1	7.1	6.5	-4.2	2.4
Continental aerosol model	2420	2.40	52.7	0.94	0.90	0.14	7.1	5.6	15.2	-3.0	12.8
Urban aerosol model	2420	2.48	45.3	0.93	0.96	0.13	2.5	5.1	5.3	0.5	-2.9

The reference LAI and C_{ab} data were generated using $\tau_{550}=0.23$ and an aerosol model consisting of 40% continental and 60% urban. See Table 2 for definition of statistical descriptors. n represents the total number of pixels included in the analysis (entire corn field).

tional REGFLEC conditions. Increasing τ_{550} to 0.31 (reference $\tau_{550}=0.23$) causes an overall increase in the LAI estimates (Bias=3.5%) and an overall decrease in the C_{ab} estimates (Bias=-3.8%) (Table 4). The relative RMS deviation between the sensitivity and reference run simulations is 8% for LAI and 10.6% for C_{ab} . The biophysical parameter retrievals are generally less impacted by running REGFLEC with $\tau_{550}=0.15$ (Table 4). The choice of aerosol model can be critical particularly for the C_{ab} estimates that increase by 12.8% if a continental aerosol model is assumed (40% continental and 60% urban was assumed for the reference conditions) (Table 4). Evidently, the setting of these parameters is quite important for accurate retrieval results. The AERONET aerosol optical depth measurements on the other hand are highly accurate (~ 0.01 uncertainty) (Holben et al., 1998) and should be used if available.

7. Discussion and conclusions

Robust biophysical parameter retrievals were effectuated using radiometric information from only 3 spectral bands (green, red and near-infrared), demonstrating that a few appropriate broad bands can be adequate for the remote sensing of vegetation biophysical and biochemical properties. Indeed, the green spectrum (around 550 nm) is recognized as being optimal for leaf chlorophyll estimation (Gitelson et al., 1996, 2005; Yoder & Pettigrew-Crosby, 1995), near-infrared reflectances are highly responsive to changing leaf biomass, canopy architecture and leaf structure (Kuusk, 2001; Bacour et al., 2002b), and the red and green reflectance difference primarily responds to changes in background reflectance and fraction of senescent vegetation (Fig. 2k and l). Broge and Mortensen (2002) showed that broadband (satellite-based) VIs were in fact slightly better at estimating LAI and leaf chlorophyll than corresponding narrow-band hyperspectral versions, and Weiss et al. (2000) found that only a limited number of wavebands were required to accurately estimate key canopy biophysical variables.

Remote estimation of leaf chlorophyll (using inverse modeling techniques) has generally been associated with fairly large uncertainties. For instance, Jacquemoud et al. (2000) reported accuracies (defined as the mean absolute difference between estimated and measured values) between 13.1 and 34.5 $\mu\text{g cm}^{-2}$ when four canopy reflectance models were inverted with airborne CASI reflectance spectra over corn and soybean with 2–5 free variables. For sugar beet, RMS deviations on the order of 10 $\mu\text{g cm}^{-2}$ were found when using AVIRIS and Landsat TM reflectance spectra (Jacquemoud et al., 1995). More recently, Botha et al. (2007) reported overall RMS deviations between 7.97 and 14.12 $\mu\text{g cm}^{-2}$ for potato cultivars by inverting PROSAIL with field measured hyperspectral data. Simulation (e.g. Combal et al., 2002a; Koetz et al., 2005) and experimental studies (Combal et al., 2002b) have demonstrated that using a priori information significantly improves the estimation accuracy of vegetation variables. While the use of a priori knowledge (i.e. canopy type and architecture, model parameter ranges) is an efficient way to solve ill-posed inverse problems, this regularization

technique typically relies on the existence of experimental data collected at the site of interest. The additional information content required to regularize the inversion must be provided by alternative means if the objective is an entirely image-based method that does not rely on impractical in-situ data and that can be used for agricultural fields characterized by widely varying distributions of model variables. The image-based regularization techniques suggested in this study resulted in LAI and C_{ab} retrieval accuracies on the order of 10% (relative RMSD). The method of exploiting the spectral information content of pixels belonging to the same land cover class was originally proposed by Atzberger (2004) who reported a significant improvement in estimation accuracies when using the neighboring radiometric information of the pixel being inverted to regularize the model inversion. Houborg and Boegh (2008) reported RMS deviations of 0.74 for LAI and $5.0 \mu\text{g cm}^{-2}$ for C_{ab} using related regularization strategies. The good agreement between the measured θ_l and the θ_l retrieved during the REGFLEC iterative inversion mode supports simulation results in Atzberger (2004) that showed that the 'object-based' approach reduced confounding effects between LAI and the leaf inclination angle. It appears that incorporating spatial (intra-field) reflectance data during model inversion help regularize the inverse problem and avoid arriving at multiple local minima caused by the interactive nature of these two geometrical parameters (Baret & Guyot, 1991; Bacour et al., 2002b).

Limiting the reflectance dataset to represent fairly dense vegetation pixels causes a decrease in the contribution of the background signal to the overall scene reflectance and an increase in the total amount of radiation scattered by plant cells (Daughtry et al., 2000) thereby improving the reliability of vegetation parameter retrievals (Botha et al., 2007; Baret & Jacquemoud, 1994). However, the NDVI threshold requirement implies that the biophysical parameters cannot be retrieved for sparsely vegetated fields with a maximum NDVI less than 0.65. In that case, image acquisitions at a more extended stage of plant development may be used to retrieve the field specific parameters (N , S_z and θ_l), assumed temporally invariant between the image acquisitions (Houborg & Boegh, 2008). Alternatively, REGFLEC can be run for sparsely vegetated fields using default values (Table 1) for N , S_z and θ_l .

Degradation in model performances is often observed during the leaf senescence stage (Bacour et al., 2002a; Wang et al., 2005). Verhoef and Bach (2003) attributed the lack of correspondence between HyMap-measured and simulated reflectance spectra in the red spectrum to the presence of yellow or brown leaves in crops assumed to consist of exclusively green leaves, and Houborg and Boegh (2008) suggested tasseling or the existence of yellow leaves as plausible reasons for underestimating LAI of a corn crop. The incorporation of the canopy fraction of senescent leaf material in REGFLEC was found to be important for matching modeled and measured reflectance spectra for a stressed corn field. There is a strong relation between f_B and the difference between red and green reflectances as increasing the amount of senescent leaf material causes an increase in red relative to green reflectance (Fig. 2). As a result f_B –RGVI relationships were found effective for the delineation of horizontal f_B gradients. However, senescent leaf reflectance spectra may vary significantly between species with variations in the brown pigment content and leaf mesophyll structure (Section 3). In addition, LAI and soil background effects (e.g. s_1) may confound the retrieval of f_B especially at low vegetation coverage (Fig. 2). Accurate pixel-wise info on s_1 is also critical as variations in background reflectance may confound the detection of relatively subtle differences in canopy reflectance due to changes in leaf chlorophyll content (Daughtry et al., 2000). Low LAI and C_{ab} estimation accuracies have been attributed to soil background interference in a number of studies (Botha et al., 2007; Qu et al., 2007), and the high LAI and C_{ab} estimation accuracies for LAI ranging from 1.5 to 4 found in this study were due in part to an effective pixel-wise correction for background effects.

In summary, the REGFLEC modeling tool that couples leaf optics (PROSPECT), canopy reflectance (ACRM), and atmospheric radiative transfer (6SV1) models demonstrated excellent LAI and C_{ab} retrieval

capabilities for a corn field characterized by a wide range in leaf chlorophyll levels. The results are especially encouraging considering the highly variable field conditions with intermixing of green and senescent leaf material and soil background interference. The generated high-resolution biophysical maps can be of high value in precision agriculture for detecting vegetation stress and fertilizer need and for crop management in general. The utility of REGFLEC for regional scale applications will soon be evaluated. For larger regions a land cover map is required to divide the image into classes that satisfy the assumption of spatially invariant leaf mesophyll structure, vegetation clumping and leaf inclination angle characteristics. The iterative inverse retrieval of the field/class-specific canopy characteristics is the most computational part of the model whereas the pixel-wise computations in the LUT-based inversion mode are much faster. This makes the computational speed of REGFLEC depend mainly on the number of land cover classes and not so much on the number of pixels (image size). Since REGFLEC is entirely image-based and is set up with wide model parameter ranges, representing diverse agricultural fields it can easily be applied to other environments and species compositions. Finally, REGFLEC is not sensor-specific but can be run at a range of spatial and temporal resolutions with radiometric information from 3 spectral bands available from airborne sensor systems such as CASI, SpecTIR, and HyMap and operational satellite sensors such as MODIS, Landsat TM/ETM+, SPOT, and MERIS.

Acknowledgements

Funding for this research was provided by the National Aeronautics and Space Administration under grant NNG04GK89G. LAI data were made available through the efforts of technician Andrew Russ of the Hydrology and Remote Sensing Lab. We would like to acknowledge the PI of the NASA GSFC AERONET site for making sun photometer data available.

References

- Anderson, M. C., Norman, J. M., Kustas, W. P., Li, F., Prueger, J. H., & Mecikalski, J. M. (2005). Effects of vegetation clumping on two source model estimates of surface energy fluxes from an agricultural landscape during SMACEX. *Journal of Hydrometeorology*, 6, 892–909.
- Atzberger, C. (2004). Object-based retrieval of biophysical canopy variables using artificial neural nets and radiative transfer models. *Remote Sensing of Environment*, 93, 53–67.
- Bacour, C., Baret, F., Beal, D., Weiss, M., & Pavageau, K. (2006). Neural network estimation of LAI, fAPAR, fCover and LAIxCab, from top of canopy MERIS reflectance data: Principles and validation. *Remote Sensing of Environment*, 105, 313–325.
- Bacour, C., Jacquemoud, S., Leroy, M., Hauteceur, O., Weiss, M., Prévot, L., et al. (2002a). Reliability of the estimation of vegetation characteristics by inversion of three canopy reflectance models on airborne POLDER data. *Agronomie*, 22, 555–565.
- Bacour, C., Jacquemoud, S., Tourbier, Y., Dechambre, M., & Frangi, J. P. (2002b). Design and analysis of numerical experiments to compare four canopy reflectance models. *Remote Sensing of Environments*, 79, 72–83.
- Baret, F. (1991). Vegetation canopy reflectance: Factors of variation and application for agriculture. In D. Hunt (Ed.), *Physical measurements and signatures in remote sensing* (pp. 145–167). France: Courchevel.
- Baret, F., & Fourty, T. (1997). Radiometric estimates of nitrogen status in leaves and canopies. In G. Lemaire (Ed.), *Diagnosis of the nitrogen status in crops* (pp. 201–227). Berlin: Springer.
- Baret, F., & Guyot, G. (1991). Potentials and limits of vegetation indices for LAI and APAR assessment. *Remote Sensing of Environment*, 35, 161–173.
- Baret, F., & Jacquemoud, S. (1994). Modeling canopy spectral properties to retrieve biophysical and biochemical characteristics. In J. Hill & J. Megier (Eds.), *Imaging Spectrometry—A Tool for environmental Observations* (pp. 145–167). ECSC, EEC, EAEC, Brussels und Luxemburg.
- Boegh, E., Soegaard, H., Broge, N., Hasager, C. B., Jensen, N. O., Schelde, K., et al. (2002). Airborne multispectral data for quantifying leaf area index, nitrogen concentration, and photosynthetic efficiency in agriculture. *Remote Sensing of Environment*, 81, 179–193.
- Botha, E. J., Leblon, B., Zebbarh, B., & Watmough, J. (2007). Non-destructive estimation of potato leaf chlorophyll from canopy hyperspectral reflectance using the inverted PROSAIL model. *International Journal of Applied Earth Observation and Geoinformation*, 9, 360–374.
- Broge, N. H., & Mortensen, J. V. (2002). Deriving green crop area index and canopy chlorophyll density of winter wheat from spectral reflectance data. *Remote Sensing of Environment*, 81, 45–57.

- Campbell, G. S. (1990). Derivation of an angle density function for canopies with ellipsoidal leaf angle distributions. *Agricultural and Forest Meteorology*, 49, 173–176.
- Campbell, G. S., & Norman, J. M. (1998). *An introduction to Environmental Biophysics* (pp. 286). New York: Springer-Verlag.
- Carter, G. A. (1994). Ratios of leaf reflectances in narrow wavebands as indicators of plant stress. *International Journal of Remote Sensing*, 15, 697–704.
- Choudhury, B. J., Ahmed, N. U., Idso, S. B., Reginato, R. J., & Daughtry, C. S. T. (1994). Relations between evaporation coefficients and vegetation indices studied by model simulations. *Remote Sensing of Environment*, 50, 1–17.
- Colombo, R., Bellingeri, D., Fasolini, D., & Marino, C. M. (2003). Retrieval of leaf area index in different vegetation types using high resolution satellite data. *Remote Sensing of Environment*, 86, 120–131.
- Combal, B., Baret, F., & Weiss, M. (2002a). Improving canopy variables estimation from remote sensing data by exploiting ancillary information. Case study on sugar beet canopies. *Agronomie*, 22, 205–215.
- Combal, B., Baret, F., Weiss, M., Trubuil, A., Macé, D., Pragnère, A., et al. (2002b). Retrieval of canopy biophysical variables from bidirectional reflectance using prior information to solve the ill-posed inverse problem. *Remote Sensing of Environment*, 84, 1–15.
- Daughtry, C. S. T., Walthall, C. K., Kim, M. S., Brown de Costoun, E., & McMurtrey, J. E., III (2000). Estimating corn leaf chlorophyll concentration from leaf and canopy reflectance. *Remote Sensing of Environment*, 74, 229–239.
- Demarez, V., Duthoit, S., Baret, F., Weiss, M., & Dedieu, G. (2008). Estimation of leaf area and clumping indexes of crops with hemispherical photographs. *Agricultural and Forest Meteorology*, 148, 644–655.
- Doraiswamy, P. C., Hatfield, J. L., Jackson, T. J., Prueger, J. H., Akhmedov, B., & Stern, A. J. (2004). Crop condition and yield simulations using Landsat and MODIS imagery. *Remote Sensing of Environment*, 92, 548–559.
- Fang, H., & Liang, S. (2005). A hybrid inversion method for mapping leaf area index from MODIS data: Experiments and application to broadleaf and needleleaf canopies. *Remote Sensing of Environment*, 94, 405–424.
- Filella, I., Serrano, L., Serra, J., & Penuelas (1995). Evaluating wheat nitrogen status with canopy reflectance indices and discriminant analysis. *Crop Science*, 35, 1400–1405.
- Gish, T. J., Dulaney, W. P., Daughtry, C. S. T., & Kung, K. -J. S. (2001). Influence of preferential flow on surface runoff fluxes. *Proceedings of the 2nd International Symposium on Preferential flow, Honolulu, Hawaii, Jan. 3–5, 2001* (pp. 205–209).
- Gitelson, A. A., Kaufman, Y. J., & Merzlyak, M. N. (1996). Use of a green channel in remote sensing of global vegetation from EOS-MODIS. *Remote Sensing of Environment*, 58, 289–298.
- Gitelson, A. A., & Merzlyak, M. N. (1997). Remote estimation of chlorophyll content in higher plant leaves. *International Journal of Remote Sensing*, 18, 2691–2697.
- Gitelson, A. A., Viña, A., Ciganda, V., & Rundquist, D. C. (2005). Remote estimation of canopy chlorophyll content in crops. *Geophysical Research Letters*, 32, L08403. doi:10.1029/2005GL022688
- Gitelson, A. A., Vina, A., Verma, S. B., Rundquist, D. C., Arkebauer, T. J., Keydan, G., et al. (2006). Relationship between gross primary production and chlorophyll content in crops: Implications for the synoptic monitoring of vegetation productivity. *Journal of Geophysical Research*, 111, D08S11. doi:10.1029/2004JD006017
- Gobron, N., Pinty, B., & Verstraete, M. M. (1997). Theoretical limits to the estimation of the leaf area index on the basis of visible and near-infrared remote sensing data. *IEEE Transactions on Geoscience and Remote Sensing*, 35(6), 1438–1445.
- Haboudane, D., Miller, J. R., Pattey, E., Zarco-Tejada, P. J., & Strachan, I. B. (2004). Hyperspectral vegetation indices and novel algorithms for predicting green LAI of crop canopies: Modeling and validation in the context of precision agriculture. *Remote Sensing of Environment*, 90, 337–352.
- Holben, B. N., Eck, T. F., Slutsker, I., Tanre, D., Buis, J. P., Setzer, A., et al. (1998). AERONET—A federated instrument network and data archive for aerosol characterization. *Remote Sensing of Environment*, 66, 1–16.
- Hosgood, B., Jacquemoud, S., Andreoli, G., Verdebout, J., Pedrini, G., & Schmuck, G. (1995). *Leaf Optical Properties Experiment 93 (LOPEX93)*, European Commission, Joint Research Centre, Institute for Remote Sensing Applications, Report EUR 16095 EN.
- Houborg, R., & Boegh, E. (2008). Mapping leaf chlorophyll and leaf area index using inverse and forward canopy reflectance modelling and SPOT reflectance data. *Remote Sensing of Environment*, 112, 186–202.
- Houborg, R., Soegaard, H., & Boegh, E. (2007a). Combining vegetation index and model inversion methods for the extraction of key vegetation biophysical parameters using Terra and Aqua MODIS reflectance data. *Remote Sensing of Environment*, 106, 39–58.
- Houborg, R., Soegaard, H., Emmerich, W., & Moran, S. (2007b). Inferences of all-sky solar irradiance using Terra and Aqua MODIS satellite data. *International Journal of Remote Sensing*, 28, 4509–4535.
- Jacquemoud, S., Bacour, C., Poilvé, H., & Frangi, J. -P. (2000). Comparison of four radiative transfer models to simulate plant canopies reflectance: Direct and inverse mode. *Remote Sensing of Environment*, 74, 471–481.
- Jacquemoud, S., & Baret, F. (1990). PROSPECT: A model of leaf optical properties spectra. *Remote Sensing of Environment*, 34, 75–91.
- Jacquemoud, S., Baret, F., Andrieu, B., Danson, F. M., & Jaggard, K. (1995). Extraction of vegetation biophysical parameters by Inversion of the PROSPECT+SAIL models on sugar beet canopy reflectance data. Application to TM and AVIRIS sensors. *Remote Sensing of Environment*, 52, 163–172.
- Kimes, D. S., Knyazikhin, Y., Privette, J. L., Abuelgasin, A. A., & Gao, F. (2000). Inversion methods for physically-based models. *Remote Sensing of Environment*, 18, 381–439.
- Kimes, D. S., & Sellers, P. J. (1985). Inferring hemispherical reflectance of the earth's surface for global energy budgets from remotely sensed nadir of directional radiance values. *Remote Sensing of Environment*, 18, 205–223.
- Knyazikhin, Y., Martonchik, J. V., Diner, D. J., Myneni, R. B., Verstraete, M., Pinty, B., et al. (1998). Estimation of vegetation canopy leaf area index and fraction of absorbed photosynthetically active radiation from atmosphere-corrected MISR data. *Journal of Geophysical Research*, 103(D24), 32239–32256.
- Koetz, B., Baret, F., Poilve, H., & Hill, J. (2005). Use of coupled canopy structure dynamic and radiative transfer models to estimate biophysical canopy characteristics. *Remote Sensing of Environment*, 95, 115–124.
- Kotchenova, S. Y., & Vermote, E. F. (2007). Validation of a vector version of the 6S radiative transfer code for atmospheric correction of satellite data. Part II: Homogeneous Lambertian and anisotropic surfaces. *Applied Optics*, 46, 4455–4464.
- Kotchenova, S. Y., Vermote, E. F., Matarrese, R., & Klemm, F. J., Jr. (2006). Validation of a vector version of the 6S radiative transfer code for atmospheric correction of satellite data. Part I: Path radiance. *Applied Optics*, 45, 6726–6774.
- Kuusk, A. (1995). A Markov chain model of canopy reflectance. *Agriculture and Forest Meteorology*, 76, 221–236.
- Kuusk, A. (2001). A two-layer canopy reflectance model. *Journal of Quantitative Spectroscopy & Radiative Transfer*, 71, 1–9.
- Kuusk, A. (2003). *Two-layer canopy reflectance model. ACRM User Guide* (pp. 21). (<http://www.aai.ee/bgf/acrm/>).
- Kuusk, A., Andrieu, B., Chelle, M., & Aries, F. (1997). Validation of a Markov chain canopy reflectance model. *International Journal of Remote Sensing*, 18, 2125–2146.
- Li, F., Kustas, W. P., Prueger, J. H., Neale, C. M. U., & Jackson, T. J. (2005). Utility of remote sensing-based two-source energy balance model under low- and high-vegetation cover conditions. *Journal of Hydrometeorology, Special Edition*, 6, 878–891.
- Lillesaeter, O. (1982). Spectral reflectance of partly transmitting leaves: Laboratory measurements and mathematical modeling. *Remote Sensing of Environment*, 12, 247–254.
- Markwell, J., Ostermann, J. C., & Mitchell, J. L. (1995). Calibration of the Minolta SPAD-502 leaf chlorophyll meter. *Photosynthesis Research*, 46, 467–472.
- Moran, S. M., Inoue, Y., & Barnes, E. M. (1997). Opportunities and limitations for image-based remote sensing in precision crop management. *Remote Sensing of Environment*, 61, 319–346.
- Moran, S. M., Maas, S. J., & Pinter, P. J., Jr. (1995). Combining remote sensing and modeling for estimating surface evaporation and biomass production. *Remote Sensing Reviews*, 12, 335–353.
- Nijs, I., Behaeghe, T., & Impens, I. (1995). Leaf nitrogen content as a predictor of photosynthetic capacity in ambient and global change conditions. *Journal of Biogeography*, 22, 177–183.
- Norman, J. M., Kustas, W. P., & Humes, K. S. (1995). A two-source approach for estimating soil and vegetation energy fluxes from observations of directional radiometric surface temperature. *Agricultural and Forest Meteorology*, 77, 263–293.
- Penuelas, J., & Filella, I. (1998). Visible and near-infrared reflectance techniques for diagnosing plant physiological status. *Trends in Plant Science*, 3, 151–156.
- Price, J. C. (1990). On the information content of soil reflectance spectra. *Remote Sensing of Environment*, 33, 113–121.
- Qu, Y., Wang, J., Wan, H., Li, X., & Zhou, G. (2007). A Bayesian network algorithm for retrieving the characterization of land surface vegetation. *Remote Sensing of Environment*. doi:10.1016/j.rse.2007.03.031
- Remer, L. A., Kaufman, Y. J., Tanre, D., Mattoo, S., Chu, D. A., Martins, J. V., et al. (2005). The MODIS aerosol algorithm, products, and validation. *Journal of the Atmospheric Sciences*, 62, 947–973.
- Richardson, A. D., Duigan, S. P., & Berlyn, G. P. (2002). An evaluation of noninvasive methods to estimate foliar chlorophyll content. *New Phytologist*, 153, 185–194.
- Tucker, C. J. (1980). Remote sensing of leaf water content in the near infrared. *Remote Sensing of Environment*, 10, 23–32.
- Uddling, J., Gelang-Alfredsson, J., Piikki, K., & Pleijel, H. (2007). Evaluating the relationship between leaf chlorophyll concentration and SPAD-502 chlorophyll meter readings. *Photosynthesis Research*, 91, 37–46.
- Verhoef, W., & Bach, H. (2003). Simulation of hyperspectral and directional radiance images using coupled biophysical and atmospheric radiative transfer models. *Remote Sensing of Environment*, 87, 23–42.
- Vermote, E. F., El Saleous, N. Z., & Justice, C. O. (2002). Atmospheric correction of MODIS data in the visible to middle infrared: First results. *Remote Sensing of Environment*, 83, 97–111.
- Vermote, E. F., & Vermeulen, A. (1999). Atmospheric correction algorithm: Spectral reflectances (MOD09). *Algorithm Technical Background Document (ATBD)* http://modis.gsfc.nasa.gov/data/atbd/atbd_mod08.pdf
- Vermote, E. F., El Saleous, N. Z., Justice, C. O., Kaufman, Y. J., Privette, J., Remer, L., et al. (1997). Atmospheric correction of visible to middle infrared EOS-MODIS data over land surface, background, operational algorithm and validation. *Journal of Geophysical Research*, 102, 17131–17141.
- Walthall, C., Dulaney, W., Anderson, M., Norman, J., Fang, H., & Liang, S. (2004). A comparison of empirical and neural network approaches for estimating corn and soybean leaf area index from Landsat ETM+ imagery. *Remote Sensing of Environment*, 92, 465–474.
- Wang, Q., Tenhunen, J., Dinh, N. Q., Reichstein, M., Otieno, D., Granier, A., et al. (2005). Evaluation of seasonal variation of MODIS derived leaf area index at two European deciduous broadleaf forest sites. *Remote Sensing of Environment*, 96, 475–484.
- Wellburn, A. R. (1994). The spectral determination of chlorophylls a and b, as well as total carotenoids using various solvents with spectrophotometers of different resolutions. *Journal of Plant Physiology*, 144, 307–313.

- Weiss, M., & Baret, F. (1999). Evaluation of canopy biophysical variable retrieval performances from the accumulation of large swath satellite data. *Remote Sensing of Environment*, 70, 293–306.
- Weiss, M., Baret, F., Myneni, R. B., Pragnère, A., & Knyazikhin, Y. (2000). Investigation of a model inversion technique to estimate canopy biophysical variables from spectral and directional reflectance data. *Agronomie*, 20, 3–22.
- Yoder, B. J., & Pettigrew-Crosby, R. E. (1995). Predicting nitrogen and chlorophyll concentrations from reflectance spectra (400–2500 nm) at leaf and canopy scales. *Remote Sensing of Environment*, 49, 81–91.
- Zarco-Tejada, P. J., Rueda, C. A., & Ustin, S. L. (2003). Water content estimation in vegetation with MODIS reflectance data and model inversion methods. *Remote Sensing of Environment*, 85, 109–124.